Modulating AP-1 enables CAR-T cells to establish an intratumoral PD-1^{+}Tcf1^{+} stem-like reservoir and overcomes resistance to PD-1 axis blockade

Authors: Andrew J. Snyder[1,2,3], Carolyn Shasha[4], Tam Ho[5], Sarah Garrison[1], Amelia R. Wilhelm[1,2,3] Mitchell G. Kluesner[1,2,3], Sergio Ortiz[1], W. Sam Nutt[1,2], Emma Bingham[1], Shruti S. Bhise[5], Everett Fan[5], Victor Zepeda[1], Megha Sarvothama[1], Xiao Wang[6], Shobha Potluri[6], Annalyssa Long[7], Anna Elz[7], Scott Furlan[5], Evan W. Newell[4], Shivani Srivastava[1,8]*

Affiliations:

[1]Human Biology Division, Fred Hutchinson Cancer Center, Seattle, Washington

[2]Molecular and Cellular Biology Graduate Program, University of Washington, Seattle, WA, USA

[3]Medical Scientist Training Program, University of Washington School of Medicine, Seattle, WA, USA

[4]Vaccine and Infectious Disease Division, Fred Hutchinson Cancer Center, Seattle, Washington

[5]Translational Science and Therapeutics, Fred Hutchinson Cancer Center, Seattle, Washington

[6]Lyell Immunopharma, South San Francisco, CA

[7]Fred Hutch Innovation Lab, Immunotherapy Integrated Research Center, Fred Hutchinson Cancer Center, Seattle, Washington

[8]Department of Immunology, University of Washington, Seattle, Washington

***Corresponding Author:** Shivani Srivastava, Fred Hutchinson Cancer Center, 1100 Fairview Avenue N, S3-204, Seattle, Washington 98109-1024

Phone: (206) 667-5103; Email: ssrivas2@fredhutch.org

Abstract:

PD-1$^+$Tcf1$^+$ stem-like cells are critical mediators of endogenous T cell responses to PD-1/PD-L1 blockade and are maintained by MHC-dependent interactions with professional antigen-presenting cells (**APCs**). Unlike conventional T cells, CAR-T cells are activated by intact antigen expressed on tumors, not by peptide/MHC expressed on APCs, restricting their activation to the hostile tumor microenvironment (**TME**) that may impair preservation of this critical stem-like subset. Indeed, in an autochthonous model of ROR1$^+$ lung cancer that we developed, CAR-T cells targeting the tumor-associated antigen ROR1 were uniformly Tcf1$^+$ prior to infusion but rapidly downregulated Tcf1 *in vivo* and became terminally exhausted, similar to observations in patients, resulting in faster attrition and no enhancement in response to PD-L1 blockade. We hypothesized that overexpression of AP-1 family transcription factors, which can regulate T cell exhaustion, could enable CAR-Ts to maintain this critical PD-1$^+$Tcf1$^+$ subset within tumors independently of APCs and sensitize them to PD-1/PD-L1 blockade. Overexpression of the AP-1 TF c-Jun, but not BATF, improved preservation of PD-1$^+$Tcf1$^+$ CAR-T cells within tumors in a cell-intrinsic manner that correlated with increased persistence deeper within tumors. Notably, c-Jun overexpression alone was insufficient to prevent CAR-T exhaustion in the lung TME, in contrast to prior work in xenograft models, with progressive CAR-T dysfunction correlated with PD-1-dependent downregulation of c-Jun. However, c-Jun overexpression dramatically sensitized CAR-Ts to PD-L1 blockade, which restored c-Jun levels in CAR-Ts, drove log-fold expansion of CAR-Ts within tumors, and induced nearly complete eradication of ROR1$^+$ tumor in highly aggressive models of lung cancer. Altogether, our data show that combination with PD-L1 blockade is necessary to unleash the full potential of c-Jun-overexpressing CAR-T cells in aggressive solid tumors like lung cancer and suggest that strategies to enhance formation of intratumoral PD-1$^+$Tcf1$^+$ reservoirs can overcome CAR-T resistance to PD-1 blockade.

Main Text:

INTRODUCTION

Immune checkpoint inhibitors (**ICI**) targeting the PD-1/PD-L1 axis have been transformative for the treatment of lung cancer, which is the leading cause of cancer mortality in the United States and worldwide,[1] but ~80% of lung cancer cases remain refractory to ICI.[2] One therapeutic strategy is to infuse patients with T cells engineered to express chimeric antigen receptors (**CAR**) specific for tumor antigens, endowing patients with a supply of functional tumor-specific T cells. Immunotherapy using CAR-T cells targeting CD19 has induced dramatic

35 remissions in some patients with advanced hematological malignancies, representing one of the
36 most remarkable therapeutic advances in the past decade.[3-12] Extending this success to more
37 common epithelial cancers like lung cancer, however, has proved more challenging.[1,13] Efficacy
38 of CAR-T cell therapies in solid tumors has been limited by multiple factors, including
39 heterogeneity of tumor antigen expression, T cell dysfunction in the tumor microenvironment
40 (**TME**), and poor persistence of infused T cells.[13-18] The tumor-associated antigen ROR1 was
41 previously identified as an attractive target for CAR-T cells due to its high expression in multiple
42 common, incurable cancers, including non-small cell lung cancer (**NSCLC**), triple-negative breast
43 (**TNBC**), and chronic lymphocytic leukemia (**CLL**), and limited expression in vital adult tissues.[19-
44 22] In a phase 1 clinical trial conducted at our Center, CAR-T cells targeting ROR1 induced
45 responses in CLL patients but upregulated multiple inhibitory receptors, became dysfunctional,
46 and persisted poorly in TNBC and NSCLC patients, suggesting that strategies to preserve CAR-
47 T function are needed to extend efficacy to more common solid tumors.[21,23] An obvious strategy
48 to rescue CAR-T cell function is to combine treatment with ICI; however, clinical studies thus far
49 have shown mixed results as to whether ICI enhances CAR-T cell efficacy, and the mechanisms
50 underlying CAR-T resistance to ICI are unclear.[24-34] Understanding the pathways that limit T cell
51 function in the context of PD-1/PD-L1 blockade, thus, is critical for developing more effective
52 immunotherapies for patients with aggressive solid tumors.

53 Recent work has demonstrated that a subset of PD-1$^+$Tcf1$^+$ exhausted T cells, termed
54 precursor exhausted cells (**Tpex**), are critical for sustaining immune responses to tumors and
55 chronic infections.[35-43] T cell exhaustion is a progressive decline in effector function and memory
56 potential driven by chronic antigen stimulation that is commonly observed in cancer and chronic
57 infection.[44-49] PD-1$^+$Tcf1$^+$ Tpex retain some stem-like qualities, including the capacity for self-
58 renewal, proliferation, and differentiation into transitory effector-like cells that mediate tumor cell
59 killing.[35-43] Tpex provide the proliferative burst after PD-1 blockade, and strategies to deplete or
60 boost Tpex can shorten or extend tumor control and response to PD-1 blockade,
61 respectively.[38,36,38,39,50,51] Unlike terminally exhausted cells , which are scattered throughout
62 tumors, Tpex preferentially co-localize with antigen-presenting cells (**APCs**) in tumor-draining
63 lymph nodes (**tdLN**) and perivascular niches, where they are maintained by MHC-dependent
64 interactions.[36,51-57] This spatial segregation has been observed in patients and multiple animal
65 models of cancer, chronic infection, and autoimmunity, suggesting that localization of Tpex to
66 APC-rich regions may protect them from terminal differentiation.[36,42,53-55,58,59] The signals provided
67 in APC niches that promote Tpex maintenance are still being uncovered and may involve

68 protection from more persistent antigen stimulation, inhibition of mTOR signaling, and/or reduced
69 hypoxia, all of which are more prevalent in the TME and promote terminal exhaustion.[39,41,50,52,60]
70 Unlike conventional T cells, CAR-T cells are primarily activated through their CAR by intact
71 antigen expressed on tumor cells, not by peptide/MHC complexes expressed on tumor cells and
72 APCs. This MHC-independent design is commonly regarded as a positive trait, as it enables CAR-
73 T cells to kill tumors that have downregulated antigen presentation on MHC, a common
74 mechanism of tumor escape from MHC-restricted T cells.[61] However, this design may also act as
75 an Achilles' heel for CAR-T cells, as it restricts their activation to the TME, a more hostile
76 environment than APC niches that may promote Tcf1 downregulation and inhibit preservation of
77 stem-like qualities. Given the critical role of APCs and tdLNs in regulating and maintaining Tpex,
78 it is unclear how insufficient activation of CAR-T cells by APCs impacts their ability to establish
79 and maintain an *in vivo* reservoir of stem-like PD-1^{+}Tcf1^{+} cells and how this affects their response
80 to PD-1 blockade.
81 Defining the mechanisms limiting CAR-T cell function and sensitivity to ICI in solid tumors
82 requires more sophisticated and rigorous animal models than are routinely in use. We previously
83 adapted the Kras$^{LSL\text{-}G12D/+}$;p53$^{fl/fl}$ (**KP**) autochthonous mouse model of NSCLC to express human
84 ROR1 (**KP^{ROR1}**) to evaluate strategies for enhancing the efficacy of ROR1 CAR-T cells.[21,62]
85 Infecting KP mice intratracheally with lentivirus expressing Cre recombinase both deletes p53 and
86 activates oncogenic Kras^{G12D} in some lung epithelial cells, resulting in development of tumors that
87 co-evolve naturally with the host immune system, develop a highly suppressive TME that
88 resembles human NSCLC, and are refractory to ICI.[62-64] We demonstrated that this aggressive
89 model recapitulates the poor persistence and dysfunction of ROR1 CAR-T cells observed in
90 patients.[21] Moreover, tumors progress slowly over 4-5 months, enabling long-term analyses of
91 CAR-T function and differentiation that are not possible in rapidly progressive transplantable and
92 xenograft models.[64] The KP^{ROR1} model, thus, closely mirrors observations in patients and provides
93 a unique platform to test strategies to enhance CAR-T cell activity and sensitivity to ICI that can
94 inform clinical translation.
95 An advantage of adoptive cell therapy is the opportunity to engineer tumor-reactive T cells
96 to promote their maintenance of PD-1^{+}Tcf1^{+} Tpex and preserve sensitivity to ICI. Exhaustion
97 develops in part due to an imbalance between NFAT and activating AP-1 transcription factors
98 (**TFs**), with insufficient activation of AP-1 TFs promoting "exhausted" rather than functional
99 "effector" T cell differentiation.[45,65] Because overexpression of AP-1 TFs have been shown to
100 regulate T cell exhaustion,[65,66] we hypothesized that modulation of AP-1 TFs could protect CAR-
101 T cells from terminal differentiation and enable them to establish an *in vivo* reservoir of stem-like

102 PD-1$^+$Tcf1$^+$ cells that could sensitize them to further enhancement with PD-1 blockade. We show
103 that, although ROR1 CAR-T cells are uniformly Tcf1$^+$ prior to infusion, they rapidly downregulate
104 Tcf1 *in vivo*, fail to establish a PD-1$^+$Tcf1$^+$ reservoir, and undergo terminal exhaustion, similar to
105 observations in patients. In the absence of a Tpex reservoir, PD-L1 blockade did not enhance
106 ROR1 CAR-T activity and instead drove their terminal differentiation and more rapid attrition within
107 tumors. Here, we use highly aggressive models of ROR1$^+$ NSCLC to define the mechanisms
108 underlying CAR-T resistance to PD-1 axis blockade and evaluate strategies to enhance formation
109 of an intratumoral reservoir of PD-1$^+$Tcf1$^+$ stem-like CAR-T cells that can restore CAR-T cell
110 sensitivity to PD-1 axis blockade.
111

112 **RESULTS**

113 ***ROR1 CAR-T cells fail to maintain a Tcf1$^+$ reservoir within lung tumors and are not***
114 ***enhanced by PD-L1 blockade***

115 We previously adapted the Kras/p53 autochthonous mouse model of lung
116 adenocarcinoma to express ROR1 by modifying the lentivirus used to induce tumors to co-
117 express Cre and truncated human ROR1 (**hROR1**).[21] Because linkage of multiple transgenes via
118 2A ribosomal skip elements can result in decreased co-expression of promoter-distal
119 transgenes,[67] we modified the lentivirus used to induce tumors to place hROR1 in the 5' position
120 (**hROR1-P2A-Cre**), which increased co-expression of Cre and hROR1 without increasing hROR1
121 levels (Fig. S1A, B).[21] In KP mice, hROR1-P2A-Cre lentivirus induced lung tumors that showed
122 hROR1 expression in ~50-70% of tumor cells by 12 weeks post-infection, when tumors were
123 visible by microCT, and this fraction remained stable up to 18 weeks post-infection (Fig. S1C).
124 Heterogeneous ROR1 expression could arise from silencing of the hROR1-P2A-Cre transgene
125 or transient Cre expression without stable lentiviral integration in a subset of cells.[68] Nevertheless,
126 this level of heterogeneity is similar to that found in patients with ROR1$^+$ TNBC and NSCLC, in
127 which ROR1$^+$ tumors express ROR1 in >50% of tumor cells.[19] The KP^{ROR1} model, thus, enables
128 us to study ROR1 CAR-T cell therapy directed against a clinically relevant antigen expressed at
129 physiological levels.

130 To target hROR1, we used a previously described ROR1 CAR comprised of a single-chain
131 variable fragment (**scFv**) that recognizes a similar epitope as the CAR used in the clinical trial
132 and CD28 and CD3ζ signaling domains (Fig. 1A).[69,70] When administered to tumor-bearing KP^{ROR1}
133 mice after lymphodepleting chemotherapy with cyclophosphamide (**Cy**), ROR1 CAR-T cells
134 accumulated within KP^{ROR1} tumors, upregulated the co-inhibitory receptors PD-1 and TIM-3, and
135 lost the ability to produce IFNγ upon restimulation *ex vivo* compared to control T cells modified to

136 express only the truncated murine CD19 transduction marker (**tCD19**) (Fig. 1A, 1B), indicating
137 that ROR1 CAR-T cells undergo terminal exhaustion in the KP^{ROR1} model.[21] Interestingly, ROR1
138 CAR-T cells prior to infusion highly expressed Tcf1, a TF critical for maintaining the stem-like
139 features of memory and Tpex cells, and did not express PD-1, exhibiting a central memory-like
140 phenotype that has been associated with improved clinical responses (Fig. 1C).[71-77] However,
141 upon infusion into tumor-bearing mice, ROR1 CAR-T cells rapidly and progressively
142 downregulated Tcf1 and upregulated PD-1, adopting a PD-1^+Tcf1^-TIM-3^+ phenotype that has
143 been associated with poor response to PD-1 axis blockade.[78] Indeed, even though ROR1 CAR-
144 T cells highly expressed PD-1 and PD-L1 was highly upregulated on tumor neutrophils and
145 macrophages in mice treated with ROR1 CAR-T cells (Fig. 1D), suggesting increased activation
146 of the PD-1/PD-L1 pathway, PD-L1 blockade did not enhance ROR1 CAR-T cell activity. While
147 PD-L1 blockade drove increased PD-1 expression and activation of ROR1 CAR-T cells, it did not
148 increase numbers of ROR1 CAR-T cells and instead drove more rapid CAR-T cell attrition within
149 KP^{ROR1} tumors (Fig. 1E). Consequently, combination treatment with anti-PD-L1 did not improve
150 ROR1 CAR-T cell efficacy, with $ROR1^+$ tumor progressing similarly in both groups (Fig. 1F, 1G).
151 Thus, despite their high expression of Tcf1 pre-infusion, ROR1 CAR-T cells fail to establish a
152 reservoir of PD-1^+Tcf1^+ cells *in vivo*, and this correlates with their terminal exhaustion and inability
153 to be enhanced by PD-L1 blockade.
154

155 ***Overexpression of AP-1 family TFs affects maintenance of intratumoral Tcf1$^+$ CAR-T cells***
156 ***and long-term persistence* in vivo**

157 We hypothesized that strategies to enhance preservation of PD-1^+Tcf1^+ CAR-T cells *in*
158 *vivo* could both improve CAR-T cell persistence and sensitize them to further enhancement with
159 ICI. T cell exhaustion is driven by a balance between NFAT and AP-1, and overexpression of AP-
160 1 family TFs like c-Jun and BATF have been shown to partially restore CAR-T cell function in
161 transplantable and xenograft tumor models.[65,66] To examine how overexpression of these AP-1
162 family TFs affected the ability of CAR-T cells to establish a PD-1^+Tcf1^+ reservoir within tumors,
163 we modified the CAR construct to co-express murine c-Jun or BATF upstream of the ROR1 CAR
164 and a tCD19/GFP transduction marker (**cJun.ROR1** and **BATF.ROR1 CAR-T cells,** respectively)
165 (Fig. 2A). Prior to infusion, cJun.ROR1 and BATF.ROR1 CAR-T cells expressed comparable
166 levels of surface CAR and higher levels of c-Jun and BATF, respectively, compared to ROR1
167 CAR-T cells (Fig. S2A). Additionally, cJun.ROR1 and BATF.ROR1 CAR-T cells showed similarly
168 high Tcf1 expression, proliferative capacity, cytokine production, and cytotoxic degranulation
169 upon stimulation as ROR1 CAR-T cells prior to infusion, though their capacity to produce IL-2 was

170 slightly increased (Fig. S2B-E). These data suggest that c-Jun or BATF overexpression do not
171 substantially alter CAR-T functional capacity prior to infusion or upon acute stimulation *in vitro*.
172 To determine how overexpression of c-Jun or BATF affected maintenance of Tcf1$^+$ CAR-T cells
173 *in vivo*, we transplanted B6 mice with lung tumors using a KP-ROR1 cell line derived from the
174 GEM model and treated them with Cy and ROR1 CAR-T, cJun.ROR1 CAR-T, or BATF.ROR1
175 CAR-T cells. Whereas tumor-infiltrating ROR1 CAR-T cells and BATF.ROR1 CAR-T cells rapidly
176 downregulated Tcf1 by 8 days post-infusion, cJun.ROR1 CAR-T cells maintained significantly
177 higher frequencies of Tcf1$^+$ cells within lung tumors, and this correlated with their significantly
178 enhanced accumulation within tumors (Fig. 2B). Correspondingly, treatment with cJun.ROR1
179 CAR-T cells, but not BATF.ROR1 CAR-T cells, induced a modest but significant extension in
180 survival compared to treatment with ROR1 CAR-T cells (Fig. 2C), suggesting that improving
181 preservation of Tcf1$^+$ CAR-T cells *in vivo* can improve tumor control.

182 Because Tcf1$^+$ Tpex have been shown to sustain and replenish T cells within tumors, we
183 next examined how c-Jun overexpression affected long-term CAR-T cell persistence *in vivo*.
184 Long-term T cell persistence, however, is difficult to assess in transplantable tumor models, in
185 which fully mature tumor cells are implanted and progress rapidly. Thus, we instead evaluated
186 how c-Jun overexpression affected CAR-T cell persistence in the autochthonous KP^{ROR1} model,
187 in which tumors progress from defined oncogenic mutations in single lung epithelial cells over 4-
188 6 months. To directly compare ROR1 CAR-T and cJun.ROR1 CAR-T cells head-to-head, we co-
189 infused a 1:1 ratio of cJun.ROR1 and ROR1 CAR-T cells into tumor-bearing KP^{ROR1} mice (Fig.
190 2D). By 7 days post-infusion, cJun.ROR1 CAR-T cells significantly outcompeted ROR1 CAR-T
191 cells at accumulating within the same KP^{ROR1} lung tumors (Fig. 2E). This competitive advantage
192 was maintained up to at least 22 days post-infusion, though both cJun.ROR1 and ROR1 CAR-T
193 cells declined in frequency over time. By contrast, both cJun.ROR1 and ROR1 CAR-T cells
194 maintained a ~1:1 ratio in spleens and lungs of non-tumor-bearing mice and in spleens of KP^{ROR1}
195 mice, suggesting that the accumulation benefit observed with c-Jun overexpression was antigen-
196 dependent. We observed similar trends when cJun.ROR1 and ROR1 CAR-T cells were infused
197 into separate mice, with cJun.ROR1 CAR-T cells showing significantly increased accumulation 8
198 days post-infusion but no significant difference by 35 days post-infusion (Fig. 2F, 2G), indicating
199 the early benefits of c-Jun overexpression were also evident in a non-competitive setting.
200 Immunohistochemistry of KP^{ROR1} lung tumors showed that cJun.ROR1 CAR-T cells persisted at
201 higher density and penetrated deeper within tumors compared to ROR1 CAR-T cells by 21 days
202 post-infusion (Fig. 2H-2I). Altogether, these data show that c-Jun overexpression significantly
203 enhances the ability of CAR-T cells to establish a PD-1$^+$Tcf1$^+$ resource population within tumors,

204 and this correlates with improved persistence deeper within tumor nests in a cell-intrinsic and
205 antigen-dependent manner; however, these benefits wane with time and result in only modestly
206 improved survival, indicating the effects of c-Jun overexpression alone are insufficient to
207 substantially enhance CAR-T cell activity in models of lung cancer.
208
209 ***c-Jun overexpression improves preservation of stem-like PD-1$^+$Tcf1$^+$ CAR-T cells within***
210 ***lung tumors in a cell-intrinsic manner***
211 Although Tcf1$^+$ cells were increased among cJun.ROR1 CAR-T cells within tumors,
212 whether this subset expresses stemness gene signatures comparable to conventional MHC-
213 restricted Tpex is not clear. To determine more comprehensively how c-Jun overexpression
214 affected CAR-T cell differentiation in the TME, we treated tumor-bearing KP^{ROR1} mice with Cy and
215 either cJun.ROR1 or ROR1 CAR-T cells and harvested lung tumors 9 days and 30 days post-
216 infusion. We used single-cell RNA sequencing (**scRNAseq**) to resolve the transcriptional profile
217 of CD8$^+$ T cells enriched from tumors at each time point, as well as of cJun.ROR1 or ROR1 CAR-
218 T cells prior to infusion. We recovered some non-T cell populations that likely reflected imperfect
219 purity of the CD8 positive selection protocol (Fig. S3A); additionally, we detected a small subset
220 of cells that exclusively expressed *Cd8, Cd4,* and *Rag1* that likely represented contaminating
221 thymocytes isolated during lung dissection, as this subset was derived from a single mouse (Fig.
222 S3B, S3C). Thus, we re-clustered the data to focus on *Cd3e*-expressing T cells and to exclude
223 contaminating thymocytes (Fig. S3D). The *CAR* transgene was highly expressed in a subset of
224 clusters, which we further sub-clustered to better resolve the transcriptional profile of CAR-T cells
225 (Fig. S3D, S3E).
226 Unsupervised clustering analysis of CAR-T cells revealed a range of cell states that
227 segregated based on time point (Fig. 3A, 3B). Cells in the CAR-T cell infusion product ("**IP**") highly
228 expressed stemness-associated genes, such as *Tcf7*, *Il7r*, and *Bach2*, and lacked expression of
229 *Pdcd1* and *Tox*, consistent with a non-exhausted central memory-like (**Tcm**) phenotype prior to
230 infusion (Fig. 3B, 3C). After infusion, a small subset of cells present at both Day 9 and Day 30
231 retained expression of central memory-like genes similar to the infusion product and likely
232 represented cells that had not yet engaged antigen *in vivo*, which we termed "**Tcm**". At Day 9, we
233 resolved 3 clusters of cells distinguished by their upregulation of the exhaustion-associated genes
234 *Pdcd1* and *Tox*. The largest of these 3 clusters expressed a combination of memory-associated
235 genes (*Tcf7*, *Il7r*, *Bach2*) and exhaustion-associated genes (*Pdcd1*, *Tox*, *Tigit*, *Lag3*), consistent
236 with the phenotype of PD-1$^+$Tcf1$^+$ stem-like precursor exhausted cells (**Tpex**) that have been
237 shown to mediate the proliferative burst in response to PD-1/PD-L1 axis blockade (Fig. 3C).[35-42,78]

238 This "**Tpex**" cluster showed strong enrichment of multiple gene signatures of PD-1^{+}Tcf1^{+} Tpex
239 derived from studies in both mouse and human T cells in chronic infection and cancer, suggesting
240 high transcriptional similarity between this CAR-T cell subset and endogenous Tpex cells (Fig.
241 3D, S3F).[38,53,78,79] We also identified a cluster of effector-like exhausted cells ("**Teff**") which
242 expressed inhibitory receptors and markers of exhaustion (*Pdcd1*, *Tox*, *Havcr2*,), lacked
243 expression of memory-like genes, and expressed the highest levels of genes associated with
244 effector function (*Ifng*, *Batf*) and costimulatory and IL-2 signaling (*Tnfsf11*, *Tnfrsf4*, *Cd70*, *Il2ra*,
245 *Stat5a*) (Fig. 3C). The final cluster enriched at Day 9 showed relatively lower expression of
246 memory-associated, effector-like, and costimulatory genes, and higher expression of inhibitory
247 receptor and exhaustion-related genes, suggesting a terminally exhausted-like phenotype ("**Tex**
248 **D9**"). By Day 30, although a small subset cells were found in the Tcm and Tpex clusters, the
249 majority of T cells were found in a cluster that lacked expression of memory- and costimulatory-
250 related genes and showed the highest expression of inhibitory receptor genes and genes
251 associated with terminal exhaustion (*Tox, Gzmk, Prf1, Eomes, Entpd1*), which we termed "**Tex**
252 **D30**" (Fig. 3C). This cluster showed strong enrichment for gene signatures of terminal exhaustion,
253 derived from both mouse and human T cells in chronic infection and cancer, that has been
254 associated with failure to respond to PD-L1 blockade (Fig. 3D, Fig. S3G).[38,53,78,79] Finally, we also
255 resolved a cluster of "**Cycling**" cells that highly expressed the cell cycle-associated genes *Mki67*
256 and *Stmn1* and was comprised of cells from each time point.

257 To compare the relative abundance of ROR1 CAR-T cells and cJun.ROR1 CAR-T cells
258 across these different cell states, we performed differential abundance testing using Milo,[80] a
259 method for differential abundance analysis across overlapping "neighborhoods". Notably,
260 cJun.ROR1 CAR-T cells were significantly enriched among 81 neighborhoods localized within the
261 Tpex cluster and defined by upregulation of the memory-associated genes *Tcf7*, *Il7r*, *Il2ra*, and
262 *Xcl1* (Fig. 3E-H). By contrast, ROR1 CAR-T cells were significantly enriched in 9 neighborhoods
263 localized within the Tex D30 cluster that were defined by upregulation of genes associated with
264 terminal exhaustion (*Eomes, Entpd1, Havcr2, Prf1, Gzmk*), indicating that ROR1 CAR-T cells
265 show more rapid terminal exhaustion while cJun.ROR1 CAR-T cells show improved preservation
266 of stem-like Tpex (Fig. 3E-H).

267 Consistent with our scRNAseq data, we used flow cytometry to validate that cJun.ROR1
268 CAR-T cells showed significantly higher frequency of PD-1^{+}Tcf1^{+}TIM-3^{-} Tpex up to 30 days post-
269 infusion, indicating that c-Jun overexpression enhanced CAR-T differentiation into Tpex *in vivo*
270 (Fig. 3I, 3J). However, Tpex frequency declined over time, suggesting progressive differentiation
271 *in vivo*. Because antigen stimulation can drive progressive differentiation,[45] we wondered whether

272 the enhanced function of cJun.ROR1 CAR-T cells might drive a reduction in ROR1^{+} tumor burden
273 that could indirectly lead to less stimulation and better preservation of Tpex. To test this, we co-
274 infused cJun.ROR1 and ROR1 CAR-T cells into tumor-bearing KP^{ROR1} mice and compared their
275 phenotype within the same tumors. cJun.ROR1 CAR-T cells maintained a higher proportion of
276 PD-1^{+}Tcf1^{+}TIM-3^{-} Tpex even in the co-infusion setting, demonstrating that enhanced Tpex
277 preservation is due to cell-intrinsic effects of c-Jun overexpression on CAR-T cells and not due to
278 extrinsic differences in the TME (Fig. 3K). Thus, our data demonstrate that c-Jun overexpression
279 enables CAR-T cells to preserve an intratumoral stem-like subset that transcriptionally resembles
280 endogenous Tpex cells.
281
282 ***c-Jun.ROR1 CAR-T cells show improved function but ultimately exhaust* in vivo**
283 Although c-Jun overexpression enabled CAR-T cells to establish a Tpex reservoir *in vivo*,
284 our scRNAseq data showed that cJun.ROR1 CAR-T cells ultimately upregulated gene signatures
285 associated with exhaustion (including *Pdcd1* and *Tox*), suggesting that c-Jun overexpression
286 alone may be insufficient to prevent exhaustion and that this may limit CAR-T cell activity *in vivo*.
287 To determine how c-Jun overexpression impacted the development of exhaustion in ROR1 CAR-
288 T cells, we analyzed the expression of co-inhibitory receptors on tumor-infiltrating CAR-T cells
289 over time, as higher and sustained levels of PD-1 and other co-inhibitory receptors is associated
290 with T cell exhaustion.[78,81-84] Nearly all CAR-T cells upregulated and maintained PD-1 expression
291 within KP^{ROR1} tumors, though cJun.ROR1 CAR-T cells upregulated PD-1 to significantly lower
292 levels and showed lower expression of TIM-3 and LAG-3 compared to ROR1 CAR-T cells 9 days
293 post-infusion (Fig. 4A, 4B). Nevertheless, cJun.ROR1 CAR-T cells eventually upregulated PD-1
294 and TIM-3 to levels comparable to ROR1 CAR-T cells by day 30 post-infusion, with only LAG-3
295 maintained at significantly lower levels. Likewise, cJun.ROR1 CAR-T cells in KP^{ROR1} tumors
296 showed higher production of IFNγ, TNFα, and IL-2 compared to ROR1 CAR-T cells within 9 days
297 post-infusion. (Fig. 4C, 4D), but this advantage was largely lost by day 35 post-infusion (Fig. 4C,
298 4D). Compared to ROR1 CAR-Ts, cJun.ROR1 CAR-T cells expressed significantly lower levels
299 of Tox, a transcription factor shown to drive and reinforce commitment to the "exhaustion"
300 program in CD8^{+} T cells (Fig. 4E, 4F)[85-88]; however, cJun.ROR1 CAR-Ts progressively
301 upregulated Tox over time, suggesting the beneficial effects of c-Jun overexpression were
302 incomplete. Notably, c-Jun overexpression showed similarly beneficial, but incomplete, effects in
303 both ROR1.BBζ and ROR1.28ζ CAR-T cells, with all treated mice showing only modestly
304 improved survival and succumbing to disease (Fig. S4). Altogether, these data indicate that c-Jun

305 overexpression is insufficient to prevent the development of exhaustion in ROR1 CAR-T cells *in*
306 *vivo*, which limits their anti-tumor activity against aggressive lung tumors.
307
308 ***c-Jun overexpression dramatically sensitizes ROR1 CAR-T cells to enhancement with PD-***
309 ***L1 blockade***
310 Although c-Jun overexpression alone did not substantially enhance ROR1 CAR-T cell-
311 mediated tumor control, we hypothesized that its ability to enhance numbers of PD-1^{+}Tcf1^{+} stem-
312 like CAR-T cells within tumors may sensitize them to enhancement with ICI. To test this, we
313 treated tumor-bearing KP^{ROR1} mice with ROR1 CAR-T or cJun.ROR1 CAR-T cells and
314 administered either blocking anti-PD-L1 antibody or vehicle every 3-4 days (Fig. 5A). By 5 days
315 post-infusion, PD-L1 blockade had no effect on ROR1 CAR-T cell numbers, as observed before,
316 but drastically boosted numbers of tumor-infiltrating cJun.ROR1 CAR-T cells >10-fold. PD-1
317 expression remained uniformly high in CAR-T cells across all treatment groups but increased
318 slightly in cJun.ROR1 CAR-T cells with PD-L1 blockade, suggesting that this combination drove
319 increased activation of cJun.ROR1 CAR-T cells (Fig.5B, 5C). Interestingly, combination treatment
320 with cJun.ROR1 CAR-T cells and anti-PD-L1 also drove a synergistic increase in numbers of
321 tumor-infiltrating endogenous CD8^{+} T cells, which also showed greater expression of PD-1,
322 suggesting that treatment with c-Jun.ROR1 CAR-T cells may also sensitize endogenous CD8^{+} T
323 cells to enhancement with PD-L1 blockade (Fig. 5C). Whereas PD-L1 blockade drove terminal
324 differentiation of ROR1 CAR-T cells (Fig 5D, 5E), it increased frequencies of both PD-1^{+}Tcf1^{+}TIM-
325 3^{-} Tpex and more differentiated PD-1^{+}Tcf1^{-}TIM-3^{+} Tex cells among cJun.ROR1 CAR-T cells,
326 suggesting an ability to both expand a stem-like reservoir and generate more differentiated
327 effector cells. Thus, c-Jun overexpression enhances ROR1 CAR-T accumulation and protects
328 them from terminal differentiation in response to PD-L1 blockade.
329
330 ***c-Jun levels are downregulated post-transcriptionally in cJun.ROR1 CAR-T cells and***
331 ***restored by PD-L1 blockade***
332 c-Jun overexpression was previously shown to prevent CAR-T cell exhaustion by
333 competing with and displacing inhibitory AP-1 transcription factors from chromatin, suggesting
334 that c-Jun levels must be sufficiently high relative to inhibitory transcription factors to mediate
335 successful reprogramming of CAR-T cells.[65] We hypothesized that incomplete prevention of
336 exhaustion in cJun.ROR1 CAR-T cells may be due to insufficiently high overexpression of c-Jun.
337 To test this, we used an antibody that detects both endogenous and transgenic murine c-Jun and
338 used flow cytometry to measure c-Jun expression in CAR-T cells over time. Whereas cJun.ROR1

339 CAR-T cells uniformly expressed higher levels of c-Jun relative to ROR1 CAR-T cells prior to
340 infusion, they significantly downregulated c-Jun levels in KP^{ROR1} tumors as early as 9 days post-
341 infusion (Fig. 6A, 6B).

342 Downregulation of c-Jun could be due to decreased transcription and/or epigenetic
343 silencing of the cJun-P2A-CAR-P2A-tCD19/GFP transgene, as retroviral vectors have been
344 reported to undergo DNA methylation in T cells *in vivo*.[89] We hypothesized that this would result
345 in equivalent downregulation of both c-Jun and the inert tCD19/GFP transduction marker encoded
346 by the retroviral transgene, such that the ratio of c-Jun to GFP protein would remain equivalent.
347 Instead, we found that the ratio of c-Jun to GFP levels decreased significantly in cJun.ROR1 CAR-
348 T cells within KP^{ROR1} tumors 9 days post-infusion relative to pre-infusion, suggesting that c-Jun
349 was being selectively downregulated relative to the tCD19/GFP marker (Fig. 6B).

350 Alternatively, high CAR expression has been shown to drive activation-induced cell
351 death[90], and because c-Jun is co-expressed with the ROR1 CAR, death of T cells with high CAR
352 (and thus high c-Jun) expression may leave behind a residual CAR-T population with lower c-Jun
353 levels. To determine whether c-Jun was selectively downregulated independently of the ROR1
354 CAR, we designed constructs which unlinked expression of c-Jun and the ROR1 CAR. We co-
355 transduced T cells with CAR-P2A-tCD19/GFP and cJun-P2A-Thy1.1 vectors and compared them
356 to T cells transduced with our standard cJun-P2A-CAR-P2A-tCD19/GFP vector (Fig. 6C). Both
357 CAR-T cells transduced with a single cJun.ROR1 CAR vector or co-transduced with separate c-
358 Jun and ROR1 CAR vectors showed equivalently high c-Jun expression prior to infusion and
359 similar downregulation of c-Jun in KP^{ROR1} tumors within 8 days post-infusion, indicating that c-Jun
360 downregulation occurred independently of co-expression with the ROR1 CAR (Fig. 6D).
361 Interestingly, although c-Jun and the Thy.1 transduction marker were highly co-expressed in the
362 pre-infusion product, <40% of $Thy1.1^{+}$ CAR-T cells maintained c-Jun expression in KP^{ROR1} tumors
363 8 days post-infusion (Fig. 6E). Thus, tumor-infiltrating cJun.ROR1 CAR-T cells downregulate c-
364 Jun independently of the ROR1 CAR and Thy1.1 or tCD19/GFP markers, suggesting that c-Jun
365 downregulation occurs post-transcriptionally.

366 c-Jun stability is regulated in part by phosphorylation by MAPK family kinases,[91] and TCR
367 signaling induces phosphorylation of c-Jun at sites that protect it from ubiquitin-mediated
368 degradation and increase its half-life.[92-96] Because of its ability to inhibit proximal TCR signaling,
369 PD-1 signaling can inhibit c-Jun phosphorylation and restrain AP-1 activity in T cell lymphomas.[97]
370 Given that PD-L1 blockade dramatically increased c-Jun CAR-T cells within KP^{ROR1} tumors, we
371 wondered whether PD-1/PD-L1 signaling was responsible for reduced c-Jun levels in cJun.ROR1
372 CAR-T cells. We treated tumor-bearing KP^{ROR1} mice with cJun.ROR1 or ROR1 CAR-T cells and

373 administered anti-PD-L1 or vehicle as before. By 5 days post-infusion, c-Jun levels were only
374 slightly, but insignificantly, elevated in cJun.ROR1 CAR-T cells relative to ROR1 CAR-T cells (Fig.
375 6F). However, treatment with anti-PD-L1 dramatically increased c-Jun levels in cJun.ROR1 CAR-
376 T cells but had no effect on ROR1 CAR-T cells (Fig. 6F), indicating that c-Jun downregulation
377 was PD-L1-dependent.

378 The effects of PD-L1 blockade on c-Jun levels in CAR-T cells could be due to direct effects
379 of disrupting PD-1 signaling in CAR-T cells and/or due to indirect effects on other PD-1^{+} or PD-
380 L1^{+} cells in the TME.[77-80] To determine whether intrinsic PD-1 signaling in CAR-T cells was
381 responsible for reduced c-Jun levels, we used CRISPR/Cas9 to selectively knockout PD-1 in
382 CD8^{+} cJun.ROR1 CAR-T cells (**cJun.ROR1$^{PD1\text{-}KO}$**) (Fig. 6G). While anti-PD-L1 drove a significant
383 increase in c-Jun levels in c-Jun.ROR1 CAR-T cells, cJun.ROR1$^{PD1\text{-}KO}$ CAR-T cells showed
384 intermediate c-Jun levels that were slightly, but insignificantly, increased compared to mock-
385 edited cJun.ROR1 CAR-T cells (Fig. 6H). To control for extrinsic differences in the TME that could
386 influence c-Jun levels, we compared c-Jun levels in mock-edited and PD-1^{KO} cJun.ROR1 CAR-T
387 cells co-infused into the same tumor-bearing KP^{ROR1} mice. Within the same tumors, PD-1^{KO}
388 cJun.ROR1 CAR-T cells showed significantly increased c-Jun levels relative to mock-edited cells,
389 though the magnitude of increase was not as large as that observed with PD-L1 blockade (Fig.
390 6I). These data suggest that c-Jun downregulation partially depends on intrinsic PD-1 signaling
391 in cJun.ROR1 CAR-T cells, but that extrinsic effects of anti-PD-L1 on other cell types likely also
392 contribute to c-Jun downregulation.
393

394 ***cJun.ROR1 CAR-T cells localize more closely to PD-L1^{+} cells and show reduced terminal***
395 ***differentiation in response to PD-L1 blockade***

396 One possible explanation for the enhanced sensitivity of cJun.ROR1 CAR-T cells to PD-
397 L1 blockade could be increased PD-1/PD-L1 signaling in tumors treated with cJun.ROR1 CAR-T
398 cells. Using scRNAseq data from live cells sorted from CAR-T cell-treated KP^{ROR1} tumors, we
399 found that among all immune cells identified, *Cd274* (which encodes PD-L1) was upregulated to
400 the greatest degree on tumor macrophages and neutrophils, which comprise the dominant
401 immune infiltrate in KP tumors (Fig. S5A-F).[98] Using flow cytometry, we confirmed that treatment
402 with ROR1 CAR-T cells and cJun.ROR1 CAR-T cells drove similarly high upregulation of PD-L1
403 on tumor cells, macrophages, and neutrophils by 9 days post-infusion compared to untreated
404 tumors (Fig. S5G), suggesting that differences in PD-L1 upregulation did not explain the vast
405 difference in CAR-T response to PD-L1 blockade.

To resolve whether ROR1 CAR-T and cJun.ROR1 CAR-T cells showed differential localization relative to various endogenous PD-L1^{+} cell types, we used the 10X Xenium spatial transcriptomics platform and designed a custom panel that included probes for genes defining various endogenous immune and stromal cells identified in our scRNA-seq data from KP^{ROR1} tumors (Fig. 3C, S5D). We also included probes for the ROR1 CAR transgene and ROR1-Cre lentiviral vector, enabling us to specifically identify *CAR*$^{+}$ T cells and *ROR1*$^{+}$ tumor cells. We treated tumor-bearing KP^{ROR1} mice with ROR1 CAR-T or cJun.ROR1 CAR-T cells, administering either vehicle or anti-PD-L1 as before, and harvested lungs from each group 7 days post-treatment to analyze by 10X Xenium. Unsupervised clustering enabled us to identify most of the cell types previously identified by scRNA-seq, including subsets of T cells, B cells, macrophages, and neutrophils (Fig. 7A, Fig. S6).

Using both the gene expression profiles and spatial coordinates of each cell, we used Leiden clustering to classify each lung into three distinct spatial regions: normal lung parenchyma, tumor, and a composite non-tumor region that included airway epithelia and blood vessels near tumor nodules (Fig. 7B). In vehicle-treated mice, ROR1 CAR-T cells were enriched within tumors, comprising ~10% of total cells within this region compared to <3% within non-tumor regions (Fig. 7B, 7C). cJun.ROR1 CAR-T cells were increased in frequency across all three spatial regions but showed preferential enrichment within tumors. Interestingly, anti-PD-L1 treatment induced a dramatic decline in ROR1 CAR-T cells across all three spatial regions, consistent with our prior data (Fig. 1D). By contrast, cJun.ROR1 CAR-T cells maintained elevated levels within tumors upon anti-PD-L1 treatment and instead showed an increase in frequency within the composite airway/blood vessel region, but not the normal lung parenchyma, that may be suggestive of increased extravasation from the circulation (Fig. 7B, 7C).

To understand how ROR1 CAR-T cells and cJun.ROR1 CAR-T cells might differ in their interactions with PD-L1^{+} endogenous cells in the TME, we mapped the localization of each cell type identified via clustering. In all treated mice, the dominant immune infiltrate within tumors was comprised of three subsets of myeloid cells that highly expressed *Cd274* (PD-L1) (Fig. 7D, S6). We identified these myeloid clusters as: 1) “M1-like macrophages”, with higher *Nos2* and lower *Tgfb1* expression; 2) “non-M1-like macrophages”, with higher *Tgfb1* and lower *Nos2* expression; and 3) neutrophils, defined by high expression of *Cxcr2, C5ar1*, and *Mmp9* (Fig. 7D, S6). Neutrophils and non-M1-like macrophages were present at highest frequency in tumors treated with ROR1 CAR-T cells; however, treatment with cJun.ROR1 CAR-T cells induced a decrease in neutrophils and non-M1-like macrophages and an increase in M1-like macrophages within tumors (Fig. 7E). As M1-like macrophages have been reported to exert anti-tumor functions,[99-103] these

440 changes suggest a polarization of the TME towards a more pro-inflammatory state. Whereas
441 addition of anti-PD-L1 to ROR1 CAR-T therapy induced a decline in M1-like macrophages,
442 addition of anti-PD-L1 to cJun.ROR1 CAR-T therapy maintained elevated frequencies of M1-like
443 macrophages, indicating that cJun.ROR1 CAR-T cells were required to enable the favorable
444 TME-remodeling effects of anti-PD-L1 on tumor macrophages.

445 We next asked whether the enhanced response of cJun.ROR1 CAR-T cells to PD-L1
446 blockade might be driven in part by increased interactions of PD-1^{+} CAR-T cells with PD-L1^{+} cells
447 within tumors. Although *Cd274*-expressing macrophages and neutrophils made up a similar
448 fraction (~60%) of all cells within tumors of mice treated with either ROR1 CAR-T cells or
449 cJun.ROR1 CAR-T cells (Fig. 7D, S6), proximity analysis revealed that PD-1^{+} cJun.CAR-T cells
450 were surrounded by significantly more PD-L1^{+} cells within a 20 um radius than PD-1^{+} ROR1 CAR-
451 T cells (Fig. 7F). These data suggest that altered spatial distribution of PD-L1^{+} cells in closer
452 proximity to cJun.ROR1 CAR-T cells may contribute to their enhanced sensitivity to enhancement
453 with PD-L1 blockade.

454 Finally, endogenous Tpex cells have been shown to be preferentially enriched in tumor-
455 draining lymph nodes and perivascular APC niches, while more terminally differentiated
456 exhausted T cells localize deeper within tumor nests.[51,53,57] Because CAR-T cells are not expected
457 to be activated by MHC-dependent interactions with APCs, we wondered whether the Tpex
458 subset formed by cJun.ROR1 or ROR1 CAR-T cells showed distinct localization from more
459 terminally differentiated subsets or whether they were able to persist deep within tumors. To
460 compare localization of Tpex CAR-T cells to other CAR-T subsets, we sub-clustered CAR-T cells
461 based on expression of genes that were most differentially expressed between CAR-T sub-
462 clusters identified from our scRNA-seq dataset (Fig. 3A, 3C). We identified subclusters that
463 correlated closely in gene expression with Tcm (*Pdcd1*^{low} *Tcf7*^{hi}), Tpex (*Pdcd1*^{hi} *Tcf7*^{hi} *Havcr2*^{lo}),
464 Teff (*Pdcd1*^{hi} *Tcf7*^{lo} *Havcr2*^{hi} *Ifng*^{hi}), and Tex (*Pdcd1*^{hi} *Tcf7*^{lo} *Havcr2*^{hi} *Ifng*^{lo} *Gzmb*^{hi}) subsets
465 identified by scRNA-seq (Fig. 7G, 7H). Treatment with cJun.ROR1 CAR-T cells induced an
466 increase in the frequency of Tpex, as well as Teff and Tex, subsets within tumors compared to
467 treatment with ROR1 CAR-T cells (Fig. 7I), consistent with our flow and scRNA-seq data.
468 Whereas anti-PD-L1 drove a similar decline in all ROR1 CAR-T cell subsets, it preferentially
469 maintained Tpex and Teff subsets and drove a decline in the Tex subset among cJun.ROR1 CAR-
470 Ts, suggesting enhanced function of cJun.ROR1 CAR-Ts. Interestingly, Tpex cells among both
471 ROR1 CAR-T cells and cJun.ROR1 CAR-T cells showed comparable intratumoral penetration to
472 more differentiated Teff cells within the same tumors, suggesting that CAR-T Tpex are not
473 spatially segregated from Teff and are capable of persisting deep within tumors. Altogether, these

474 data suggest that c-Jun overexpression protects ROR1 CAR-T cells from terminal exhaustion and
475 attrition induced by PD-L1 blockade.
476
477 ***c-Jun overexpression overcomes resistance of ROR1 CAR-T cells to PD-L1 blockade***
478 To determine whether combination therapy with cJun.ROR1 CAR-T cells and PD-L1
479 blockade was sufficient to enhance tumor control, we treated tumor-bearing KP^{ROR1} mice with
480 ROR1 CAR-T or cJun.ROR1 CAR-T cells and administered either vehicle or anti-PD-L1 every 3-
481 4 days for a total of 14 days (5 total doses) (Fig. 8A). Four weeks after cessation of anti-PD-L1
482 treatment, we harvested lungs and used immunohistochemistry to quantify $ROR1^+$ tumor burden.
483 Treatment with ROR1 CAR-T cells showed minimal reduction in $ROR1^+$ tumor burden relative to
484 untreated KP^{ROR1} mice, with the majority of tumors maintaining ROR1 expression (Fig. 8B, 8C).
485 Treatment with cJun.ROR1 CAR-T cells alone showed a slight but insignificant decrease in
486 $ROR1^+$ tumor burden compared to treatment with ROR1 CAR-T cells, consistent with the transient
487 improvement in cJun.ROR1 CAR-T cell function and the modest improvement in survival we
488 observed in transplantable models of lung cancer. Whereas PD-L1 blockade had no significant
489 effect on tumor control by ROR1 CAR-T cells and even slightly worsened it (Fig. 8C), it
490 dramatically improved tumor control by cJun.ROR1 CAR-T cells, with $ROR1^+$ tumor eliminated in
491 nearly all treated mice. Total tumor was also significantly decreased in mice treated with
492 cJun.ROR1 CAR-T cells and anti-PD-L1 relative to mice treated with ROR1 CAR-T cells and anti-
493 PD-L1 (Fig. 8C). However, $ROR1^-$ tumor continued to progress in mice treated with cJun.ROR1
494 CAR-T cells and anti-PD-L1, suggesting escape of antigen-null tumor may limit efficacy.
495 To test whether escape of $ROR1^{null}$ tumor is the major factor limiting efficacy of cJun.ROR1
496 CAR-T and anti-PD-L1 combination therapy, we evaluated this treatment regimen in a lung tumor
497 model with less pre-existing heterogeneity and more uniform expression of ROR1. We induced
498 lung tumor development in B6 mice by intravenously injecting a KP-ROR1 cell lined derived from
499 the GEM model which had been sorted to ensure >95% positivity for ROR1 (Fig. 8D, 8E).
500 Strikingly, in this setting with more uniform ROR1 expression on tumors, PD-L1 blockade again
501 had no effect on numbers of tumor-infiltrating ROR1 CAR-T cells but boosted cJun.ROR1 CAR-
502 T cells numbers within tumors ~100-fold (Fig. 8F, 8G). Although endogenous $CD8^+PD\text{-}1^+$ T cells
503 were increased ~5-fold by treatment with ROR1 CAR-T cells and anti-PD-L1 together compared
504 to treatment with ROR1 CAR-T cells alone, their numbers increased ~100 fold upon treatment
505 with cJun.ROR1 CAR-T cells and anti-PD-L1, suggesting a synergistic increase in activation of
506 endogenous T cells by this combination. In contrast to results in the GEM model, addition of anti-
507 PD-L1 to ROR1 CAR-T cell treatment showed a slight improvement in survival, though these

effects were likely driven by increases in endogenous CD8$^+$ T cells, as numbers of ROR1 CAR-T cells were unchanged by anti-PD-L1 treatment (Fig. 8F, 8G). However, treatment with cJun.ROR1 CAR-T cells and anti-PD-L1 together significantly improved survival compared to all other treatment groups (Fig. 8H). Altogether, our data demonstrate that c-Jun overexpression dramatically reverses CAR-T cell resistance to PD-L1 blockade, enabling efficient regression of ROR1$^+$ tumors and improved survival in aggressive models of ROR1$^+$ lung cancer.

DISCUSSION

PD-1$^+$Tcf1$^+$ Tpex cells are critical for sustaining endogenous anti-tumor immune responses to PD-1/PD-L1 blockade, but whether CAR-T cells can maintain this critical resource population *in vivo* and how this affects their sensitivity to ICI have not been well-defined. Here, we demonstrate that, despite showing high Tcf1 expression, polyfunctionality, and expression of stemness gene signatures prior to infusion, ROR1 CAR-T cells rapidly downregulate Tcf1 and are unable to establish a PD-1$^+$Tcf1$^+$ stem-like reservoir *in vivo*, resulting in rapid terminal exhaustion and faster attrition in response to PD-L1 blockade. Overexpression of the AP-1 family TF c-Jun, but not BATF, significantly improved preservation of PD-1$^+$Tcf1$^+$ stem-like CAR-T cells within tumors in a cell-intrinsic manner and sensitized CAR-T cells to enhancement with ICI, enabling nearly complete elimination of ROR1$^+$ tumor and improved survival in highly aggressive models of ROR1$^+$ lung cancer. Notably, c-Jun overexpression alone was insufficient to prevent CAR-T exhaustion in the lung TME, in contrast to prior work in xenograft models, with progressive CAR-T dysfunction correlated with PD-1-dependent downregulation of c-Jun. PD-L1 blockade restored c-Jun levels, suggesting that PD-1 axis inhibition may be necessary to reveal the full potential of c-Jun-overexpressing CAR-T cells in the suppressive microenvironment of aggressive solid tumors like lung cancer. Altogether, our data show that ROR1 CAR-Ts fail to establish an intratumoral PD-1$^+$Tcf1$^+$ stem-like reservoir, but that c-Jun overexpression can overcome this defect and may serve as a readily translatable strategy to sensitize previously refractory CAR-Ts to PD-1 axis blockade.

Although ICI can rescue endogenous anti-tumor activity and has been transformative for the treatment of many solid tumors,[104,105] combination of CAR-T therapy with ICI has shown mixed result in patients, and the mechanisms underlying CAR-T resistance to ICI are unclear.[24-34] Our data suggest that the ability of CAR-T cells to establish and maintain a PD-1$^+$Tcf1$^+$ stem-like reservoir *in vivo* is a critical determinant of sensitivity to ICI. Although Tcf1 expression and stemness in cell therapy infusion products is associated with improved clinical responses,[71-77] signals within the TME may promote terminal differentiation of infused cells and fail to protect a

542 subset of stem-like CAR-T cells that can sustain anti-tumor responses and expand in response
543 to PD-1/PD-L1 blockade. Indeed, signals known to protect endogenous stem-like Tpex cells, such
544 as MHC-I-dependent interactions with DCs in APC niches and tumor-draining lymph nodes,[51,52,57]
545 are likely bypassed by CAR-T cells, which do not depend on peptide/MHC for activation. Thus,
546 CAR-T cells may be uniquely disadvantaged at establishing this critical stem-like reservoir *in vivo*,
547 which may contribute to their poor persistence, exhaustion, and resistance to PD-L1 blockade.[47]
548 Indeed, despite showing high Tcf1 expression and polyfunctionality prior to infusion, ROR1 CAR-
549 T cells rapidly downregulated Tcf1 *in vivo* and showed increased terminal differentiation and more
550 rapid attrition in response to PD-L1 blockade, potentially even worsening tumor control. These
551 results mirror those shown in recent studies where depletion of DCs or knockout of MHC-I
552 expression on DCs drove terminal differentiation of Tpex cells and loss of viral control,[51,57]
553 suggesting that absence of MHC-I-dependent interactions with DCs may drive rapid terminal
554 differentiation of CAR-T cells *in vivo*. Importantly, our data suggest that overexpression of c-Jun
555 may be one strategy that bypasses these limitations and enables CAR-T cells to establish an
556 intratumoral stem-like reservoir that can sensitize them to enhancement with ICI. Notably, c-Jun
557 overexpression did not substantially increase Tcf1 expression or functionality of ROR1 CAR-T
558 cells prior to infusion; however, it may protect CAR-T cells from signals they receive in the TME
559 that promote their terminal differentiation and downregulation of Tcf1. Interestingly, cJun.ROR1
560 CAR-T cells showed significantly better preservation of Tpex within tumors even when co-infused
561 with ROR1 CAR-T cells into the same tumor-bearing mice, indicating that c-Jun overexpression
562 enhances preservation of this critical stem-like subset in a cell-intrinsic manner. Although the
563 mechanisms by which c-Jun promotes differentiation of stem/memory-like Tcf1^{+} subsets are
564 unclear, some studies suggest that c-Jun can directly bind to the *Tcf7* locus and disrupt binding
565 of inhibitory AP-1 TFs like IRF4, which promote CD8^{+} T cell exhaustion and impair memory
566 development during chronic infection.[65,106] Interestingly, endogenous Tpex cells also show strong
567 enrichment for c-Jun DNA binding,[41] and a recent study demonstrated that neuropilin-1 induced
568 c-Jun down-regulation in endogenous tumor-specific T cells that correlated with poor Tpex self-
569 renewal, terminal differentiation, and resistance to ICI.[107] These data suggest that c-Jun levels
570 may broadly correlate with sensitivity to ICI among both endogenous and engineered T cells.[65,108-
571 111]

572 Since the initial study by Lynn et al. showing that c-Jun overexpression renders CAR-T
573 cells “exhaustion resistant” in xenograft models, there has been limited demonstration that c-Jun
574 overexpression is sufficient to enhance CAR-T activity in patients or more clinically relevant
575 mouse models, and the mechanisms limiting c-Jun activity *in vivo* have not been defined.[65,66,112]

576 Indeed, preliminary data from a phase 1 clinical trial evaluating ROR1 CAR-T cells overexpressing
577 c-Jun indicate that c-Jun overexpression increases the anti-tumor activity and stem-like properties
578 of ROR1 CAR-T cells in patients with ROR1^{+} TNBC and NSCLC but is insufficient to mediate
579 complete responses, mirroring our results in the KP^{ROR1} model.[113] Our data suggest that PD-1/PD-
580 L1-dependent downregulation of c-Jun is a major factor limiting efficacy of c-Jun.ROR1 CAR-T
581 cells, and this down-regulation may be more pronounced in tumors heavily infiltrated by PD-L1^{+}
582 myeloid cells. Indeed, our data show that, similar to human NSCLC and in contrast to xenograft
583 models, macrophages and neutrophils comprise the dominant immune infiltrate within KP^{ROR1}
584 tumors, highly express PD-L1, and co-localize closely with PD-1^{+} CAR-T cells.[114,115] Thus,
585 myeloid-derived PD-L1 could contribute to increased PD-1 signaling, c-Jun down-regulation, and
586 ultimate cJun.ROR1 CAR-T dysfunction that is observed in immune-competent models but not
587 xenograft models, which lack PD-L1^{+} myeloid cells.[116] Although the mechanisms by which the
588 PD-1/PD-L1 axis down-regulates c-Jun in CAR-Ts is unclear, our data indicate that c-Jun down-
589 regulation depends partially on intrinsic PD-1 signaling within CAR-T cells. PD-1 signaling may
590 inhibit c-Jun phosphorylation at sites that prevent binding to E3 ubiquitin ligases, resulting in
591 increased ubiquitin-mediated degradation.[92-97] In fact, PD-1 signaling has been shown to activate
592 ubiquitin ligases that facilitate degradation of critical components of the TCR and IL-2 signaling
593 pathways, driving T cell dysfunction.[117-119] Altogether, our data reveal that PD-L1 blockade
594 significantly restores c-Jun levels and cJun.ROR1 CAR-T cell activity *in vivo*, providing a readily
595 translatable strategy to maximize the benefits of c-Jun overexpression in patients.

596 The KP model is notoriously aggressive, and achieving nearly complete elimination of
597 ROR1^{+} tumor with a single infusion of CAR-T cells and only two weeks of anti-PD-L1 treatment is
598 a major feat. However, our data also indicate that efficacy is likely to be limited by progression of
599 ROR1^{null} tumor. As most targets for CAR-T cells in solid tumors are heterogeneously expressed,
600 escape of antigen^{null} tumor is likely to impair efficacy of even the most potent CAR-T cell products.
601 One limitation of the KP^{ROR1} model is that the ROR1 expressed within tumors is truncated and
602 does not signal. As ROR1 has been shown to play a functional role in promoting tumor
603 proliferation, growth, and metastasis,[19,120-128] there may be a greater selective pressure against
604 escape of ROR1^{null} tumors in patients that is not appropriately modeled in KP^{ROR1} mice.
605 Nevertheless, strategies to control escape of antigen^{null} tumors will be critical for efficacy of CAR-
606 T therapy in patients with heterogeneous solid tumors. One approach is to engage the
607 endogenous anti-tumor immune response, which may be polyclonal and capable of controlling
608 escape of tumors that lack or downregulate expression of the CAR target. Our studies show that
609 combination of c-Jun CAR-T cells with PD-L1 blockade synergistically boosted numbers of

610 endogenous PD-1^{+} CD8^{+} T cells within KP tumors, though whether these cells contribute to tumor
611 control is not known. As KP tumors lack the high mutational burden of human NSCLC tumors,[129]
612 additional studies introducing model neoantigens into KP tumors may be needed to determine
613 whether combination of c-Jun CAR-T cells with PD-L1 blockade can synergistically activate
614 endogenous tumor-specific immune responses to control escape of CAR antigen^{null} tumors.
615 Finally, while c-Jun overexpression significantly enhances CAR-T cell function and
616 response to ICI, it is possible that enhanced CAR-T cell activity may reveal new toxicities *in vivo*.
617 ROR1, like most target antigens for CAR-T cells in solid tumors, shares some expression in
618 normal tissues, including parathyroid, pancreatic islets, and gastric mucosa.[19] As the CAR used
619 in our study targets human ROR1 in KP tumors and does not cross-react with murine ROR1, we
620 are unable to evaluate the effects of c-Jun CAR-T therapy and PD-L1 blockade on on-target off-
621 tumor toxicity in this model.[21,22] Although ROR1 CAR-T cells did not induce dose-limiting toxicities
622 in patients with ROR1^{+} CLL, TNBC or NSCLC, 67% of patients experienced reversible grade 3 or
623 4 pulmonary adverse events, suggesting that lung tissue may be susceptible to toxicity.[23] Notably,
624 despite the massive accumulation of c-Jun.ROR1 CAR-T cells in the lung upon PD-L1 blockade,
625 we did not observe any toxicity in the KP^{ROR1} model, suggesting that efficacy and safety can be
626 balanced in the absence of CAR target expression on normal tissue. Strategies to enhance CAR-
627 T cell activity, thus, may need to be coupled with logic-gating strategies to restrict CAR-T cell
628 activity to tumor cells to enhance anti-tumor activity without compromising safety. Alternatively,
629 antigens with heterogeneous but tumor-specific expression, like EGFRvIII or the Tn-Muc1
630 glycoform,[130,131] may be attractive candidates to target in combination with c-Jun overexpression
631 and/or PD-L1 blockade, as our data show that this treatment strategy significantly reduced tumor
632 burden without toxicity despite ROR1 being expressed in only ~60% of tumor cells prior to CAR-
633 T infusion.
634 In summary, our data demonstrate that c-Jun overexpression enables ROR1 CAR-T cells
635 to establish a critical stem-like reservoir *in vivo* that dramatically sensitizes them to enhancement
636 with PD-L1 blockade, providing a strong rationale for combining c-Jun CAR-T cell therapy with
637 ICI to enhance efficacy in patients. Moreover, given that c-Jun levels correlate broadly with
638 sensitivity of both endogenous and engineered T cells to ICI, our work raises the exciting
639 possibility that c-Jun overexpression could be broadly applied to sensitize not only CAR-T, but
640 also TCR-T and tumor-infiltrating lymphocyte (**TIL**) adoptive cell therapies, to enhancement with
641 ICI. Such strategies to sensitize endogenous and engineered T cells to ICI have the potential to
642 extend the transformative benefits of ICI to the majority of cancer patients who remain refractory
643 to ICI.

644 **MATERIALS AND METHODS**

645

646 **EXPERIMENTAL MODEL AND SUBJECT DETAILS**

647 *Animals*

648 C57BL/6 (**B6**) and B6.SJL (**CD45.1**) mice were purchased from Jackson Laboratory. *Kras*$^{LSL-}$
649 $^{G12D/+}$*;p53*$^{fl/fl}$ (**KP**) mice were generously provided by A. McGarry Houghton (FHCC, Seattle WA).
650 For studies with KP mice, 8-18 week old age-matched and sex-matched mice were used. For all
651 other studies, 8-12 week old age-matched and sex-matched mice were used. Mice of the same
652 sex were randomly assigned to experimental groups or were assigned based on tumor burden
653 such that all experimental groups had similar average tumor volume prior to treatment. All mice
654 were housed and bred at the FHCC (Seattle, WA). All experiments were performed in accordance
655 within the guidelines of the FHCC Institutional Animal Care and Use Committee
656 (PROTO202000031).

657

658 *Cell Lines*

659 The KP1233 ("KP") tumor and 3TZ "GreenGo" cell lines were generously provided by Tyler Jacks
660 (Massachusetts Institute of Technology). KP-ROR1 tumor cell lines were previously described[21]
661 and were generated by retroviral transduction of the KP tumor cell line with full-length human
662 ROR1 (UniProt: Q01973) and subsequent FACS sorting of ROR1^{+} cells to >95% purity. All cells
663 were tested bi-monthly for the absence of mycoplasma. KP, KP-ROR1, and 3TZ cell lines were
664 maintained in complete DMEM (DMEM with 10% FBS, 2mM L-glutamine, 100U/ml
665 penicillin/streptomycin, 25mM HEPES). Lenti-X cells for lentiviral packaging were purchased from
666 Clontech. Plat-E cells for retroviral packaging were purchased from Cell Biolabs. All cells were
667 tested bi-monthly for the absence of mycoplasma. KP, KP-ROR1, 3TZ, Plat-E, and LentiX cell
668 lines were maintained in complete DMEM (DMEM with 10% FBS, 2 mM L-glutamine, 100 U/ml
669 penicillin/streptomycin, 25 mM HEPES).

670

671 **METHOD DETAILS**

672 *Cloning of Murine CAR Constructs*

673 The MP71 retroviral vector, which was a gift from W. Uckert (Max Delbruck Center for Molecular
674 Medicine), was modified to encode a human ROR1-specific CAR co-expressed with a truncated
675 murine CD19 transduction marker (**tCD19**). In some experiments, the tCD19 transduction marker
676 was fused to eGFP (tCD19/GFP). The ROR1 CAR possessed a murine CD8α signal peptide
677 (UniProt: P01731, aa1-27), 2A2 scFv[21,132], human IgG4 short spacer[133], murine CD28

678 transmembrane (UniProt: P31041, aa151-177), murine 4-1BB signaling domain (UniProt:
679 P20334, aa211-256) or murine CD28 signaling domain with an LL→GG substitution located at
680 positions 184-185 of the native CD28[134] (UniProt: P31041, aa178-218), murine CD3ζ (UniProt:
681 P24161, aa52-164), and was linked by a P2A ribosomal skip element to tCD19/GFP. To generate
682 ROR1 CARs co-expressing c-Jun or BATF, the vector was further modified to express murine c-
683 Jun (Uniprot: P05627) or murine BATF (Uniprot: O35284) upstream and linked by a P2A skip
684 element to ROR1 CAR-P2A-tCD19/GFP. To generate the cJun-P2A-Thy1.1 vector, murine c-Jun
685 (Uniprot: P05627) was linked by a P2A skip element to Thy1.1 (Uniprot: P01831). Vectors
686 expressing only the tCD19 or tCD19/GFP marker was used to generate control T cells.
687
688 *Generation of Murine CAR-T Cells*
689 Retrovirus was produced by transient transfection of Plat-E cells with the indicated MP71 vectors.
690 Viral supernatant was harvested 48 hr after transfection, filtered through a 0.45 µm pore filter, and
691 snap-frozen in liquid nitrogen for long-term storage. Cell suspensions were prepared from spleen
692 and peripheral lymph nodes of donor mice by tissue disruption with glass slides and filtered
693 through a 40 µm filter. Murine $CD8^+$ and $CD4^+$ T cells were enriched from spleens and peripheral
694 lymph nodes of donor mice using untouched negative isolation kits (Stem Cell) and stimulated
695 with anti-CD3/28 Mouse T-Activator Dynabeads (ThermoFisher) at a bead to cell ratio of 1:1 for
696 24 hr in a 37°C, 5% CO_2 incubator in complete RPMI (RPM1 1640, 10% heat inactivated FBS, 1
697 mM sodium pyruvate, 1 mM HEPES, 100 U/ml penicillin/streptomycin, 50 µM β-mercaptoethanol)
698 supplemented with 50 U/ml recombinant human IL-2 (Peprotech). Non-tissue culture plates were
699 coated with 12.5 µg/ml RetroNectin (TaKaRa) according to the manufacturer's protocol, and
700 plates were loaded with pre-titered virus per well and centrifuged for 2 hr at 3000xg at 32°C. For
701 co-transduction experiments, pre-titered virus was mixed 1:1 and added to pre-coated
702 RetroNectin wells and centrifuged for 2 hr at 3000xg. Murine T cells were harvested and
703 resuspended at $1x10^6$ cells/ml in fresh complete RPMI supplemented with 50 U/ml IL-2. Viral
704 supernatant was aspirated from RetroNectin-coated plates, plates were rinsed with PBS, and T
705 cells were added to each virus-coated well. Plates were then centrifuged at 800g for 30 min at
706 32°C and returned to 37°C, 5% CO_2 incubators. After 24 hours, T cells were harvested and
707 resuspended in complete RPMI with 50 U/ml IL-2. T cells were subsequently harvested, counted,
708 and maintained at $1x10^6$ cells/ml in complete RPMI with 50 ng/ml human IL-15 every 1-2 days
709 after. Four days after transduction, magnetic beads were removed and T cell transduction was
710 measured by flow cytometry staining for tCD19, GFP, Thy1.1, ROR1 CAR, and/or c-Jun.
711 Transduced cells were enriched using the EasySep CD19 Positive Selection Kit II (Stem Cell)

712 and either used immediately for *in vitro* or *in vivo* experiments or cryopreserved in complete RPMI
713 supplemented with 10% FBS and 10% DMSO. Cryopreserved cells were thawed in a 37°C water
714 bath, washed, counted, re-confirmed for viability, tCD19, GFP, Thy1.1, ROR1 CAR, and/or c-Jun
715 expression by flow cytometry, and used immediately for experiments.
716
717 *Generation of PD-1^{KO} CAR-T cells*
718 Ribonucleoprotein (**RNP**) complex was prepared by combing PD1-sgRNA (5′-
719 ACAGCCCAAGUGAAUGACCA) and Cas9 protein (Horizon Cat# CAS12206) at a 3:1 molar ratio.
720 Lonza P3 buffer (Catalog #: V4XP-3024) was prepared according to package insert. Murine CD8$^+$
721 T cells were isolated from spleens and peripheral lymph nodes of donor mice and stimulated with
722 anti-CD3/28 Mouse T-Activator Dynabeads (ThermoFisher) at a bead to cell ratio of 1:1 for 24 hr
723 in a 37°C, 5% CO_2 incubator in complete RPMI supplemented with 50 U/ml recombinant human
724 IL-2, as described above. After 24 hr of stimulation, CD8$^+$ T cells were harvested, de-beaded, and
725 resuspended in Lonza P3 buffer and RNP (4x10^6 cells per 80 ul). The cell/RNP mixture was
726 transferred to a Lonza 4D-Nucleofector® X Kit L cuvette (Catalog #: V4XP-3024) and
727 electroporated in a Lonza 4D Nucleofector Core Unit using the "CA137" program. Following
728 electroporation, cells were rested at 37°C for 15 mins. Mouse T-Activator anti-CD3/28 beads were
729 added back to the cell suspension 1:1 with T-cells. T cells were then added to retrovirus-coated
730 plates and cultured as described above. Five days post-electroporation, genomic DNA (**gDNA**)
731 was extracted from a subset of cells using the QuickExtract™ DNA Extraction Solution
732 (BioScience Technologies, QE0905T). The 900 bp region surrounding the sgRNA was amplified
733 via PCR with forward (5'-CACCTCTAGTTGCCTGTTCT) and reverse (5'-
734 CACCTGTAAAACCCACCTAA) primers. gDNA was sequenced by ACGT DNA Sequencing
735 Services, using the primer sequence CACCTCTAGTTGCCTGTTCT. Indel frequencies were
736 determined using the ICE analysis tool provided by Synthego Corporation. To further validate
737 efficient knockdown of PD-1 expression, T cells were stimulated with 50ng/ml PMA and 1 µg/ml
738 ionomycin in 0.2 ml complete RPMI in 96-well U-bottomed plates (Costar) at 37°C, 5% CO_2 for
739 24 hr and analyzed by flow cytometry for expression of PD-1 by flow cytometry.
740
741 *Generation, Titration, and Intratracheal Administration of Cre Lentivirus*
742 We previously described modification of the HIV7 lentiviral vector[135] to encode Cre
743 recombinase, firefly luciferase (**ffluc**), and truncated human ROR1 (**hROR1t**) (UniProt: Q01973,
744 aa 1-462), with each transgene linked by P2A and T2A ribosomal skip elements (Cre-P2A-ffluc-
745 T2A-hROR1t).[21] We further modified this vector to reposition hROR1t in the 5' position, by

746 expressing hROR1t (UniProt: Q01973, aa 1-462) linked by a P2A ribosomal skip element to Cre
747 recombinase (**hROR1-P2A-Cre**). As a control, the HIV7 vector was modified to express Cre only.
748 Lentivirus was produced by transient calcium phosphate transfection of the packaging cell
749 line LentiX with the indicated HIV7 lentiviral vectors, psPAX2 (Addgene #12260), and VSVg
750 envelope. Viral supernatant was harvested 24, 48 and 72 hr after transfection, filtered through a
751 0.45-µm pore filter, and stored at 4°C for up to 1 week until ready for ultracentrifugation. Lentivirus
752 was concentrated by mixing filtered lentivirus with 40% polyethylene glycol (PEG, Sigma) at a
753 PEG to virus ratio of 1:3 for 12-24 hr at 4°C. The virus/PEG mixture was then centrifuged at 1500g
754 for 45 min at 4°C, supernatant was aspirated, and the virus pellet was resuspended in 30 ml
755 serum-free DMEM. Lentivirus was further concentrated in an Optima L-90K ultracentrifuge
756 (Beckman Coulter) at 24,500 rpm for 90 min at 4°C. The final virus pellet was resuspended in 0.5
757 – 1 ml serum-free DMEM by vortexing for 1-3 hr at 4°C, aliquoted, and frozen at -80°C for long-
758 term storage.
759 Cre lentivirus was titered using 3TZ "Green Go" cells. Briefly, $5x10^4$ 3TZ cells were plated
760 in 1 ml of complete DMEM in 12-well plates. 5-6 hours later when cells were adherent, supernatant
761 was aspirated and media was replaced with 0.5 ml complete DMEM containing serial dilutions of
762 thawed Cre lentivirus (e.g. 10-fold serial dilutions from 1:10 to 1:10,000) and 8 µg/ml polybrene.
763 After 24 hr, media was replaced with 1 ml complete DMEM and cells were passaged for 3-4 days
764 before analysis by flow cytometry for GFP and/or hROR1 expression. Virus titer was calculated
765 according to the following formula: Titer (pfu/µl) = [($5x10^4$) * (%GFP^+ cells) / 100] / [Volume of
766 virus added (µl)]. Lung tumors were induced in KP mice by intratracheal intubation and inhalation
767 of $2x10^4$ pfu Cre-expressing lentivirus as reported.[62]
768
769
770 *CAR-T Cell Treatment of KP^{ROR1} mice*
771 KP mice were scanned by micro-computed tomography (micro-CT) ~10-11 weeks post-infection
772 and one week before T cell infusion, and tumor burden was calculated for each mouse using 3D
773 Slicer image computing platform. Mice were distributed into treatment groups such that the
774 average tumor burden was as similar as possible prior to treatment to control for variability in
775 induction of tumors. For all T cell infusion experiments, KP mice were injected intraperitoneally
776 with 150 mg/kg cyclophosphamide and 6-24 hr later were injected intravenously by retro-orbital
777 injection with $6×10^6$ live $tCD19^+$ control or CAR-T cells (1:1 ratio of CD8:CD4 T cells). For co-
778 transfer experiments, ROR1 CAR-T and cJun.ROR1 CAR-T cells were mixed 1:1 prior to infusion.
779 Mice were monitored for weight, body condition score, tumor burden, and survival where

780 indicated. All mice in each experiment were sacrificed when any individual mice showed clinical
781 signs of severe disease or 20 percent weight loss.
782
783 *Lung Metastatic Transplantable KP Tumor Model*
784 5×10^4 KP-ROR1 tumor cell lines were injected intravenously via tail vein into 8–12 week old B6
785 mice to induce development of metastatic lung tumors. After 21 days, tumor-bearing mice were
786 injected intraperitoneally with 150 mg/kg cyclophosphamide and 6-24 hr later were injected with
787 6×10^6 live $tCD19^+$ control or CAR-T cells (1:1 ratio of CD8:CD4 T cells). Mice were monitored for
788 weight, body condition score, tumor burden, and survival where indicated. All mice in each
789 experiment were sacrificed when any individual mice showed clinical signs of severe disease or
790 20 percent weight loss.
791
792 *Anti-PD-L1 Treatment*
793 In some experiments, mice were treated with 200 ug anti-PD-L1 antibody (BioXcell, clone:
794 10F.9G2) intraperitoneally every 3-4 days beginning 1 day post T cell transfer and continuing for
795 14 days (5 total doses).
796
797 *Preparation of Tissues for Flow Cytometry and RNAseq*
798 Cell suspensions were prepared from murine spleen and peripheral lymph nodes by tissue
799 disruption with glass slides and filtering through a 40 µm filter, and lysing with ACK lysis buffer
800 (Gibco). For analysis of lung tumors, mice were injected with 400 ng PECy7-conjugated anti-
801 CD45 antibody (clone 30-F11, BioLegend) intravenously via retro-orbital injection 5 min prior to
802 euthanasia to distinguish vascular and non-vascular cells in the lung. Whole lungs were placed in
803 GentleMACS C Tubes with 6 ml of complete RPMI supplemented with 2 mg/ml collagenase IV
804 (Worthington) and 80 U/ml DNAse I (Worthington). Lungs were minced using the
805 "m_impTumor_01_01" program on a GentleMACS Octo Dissociator and incubated in a 37°C
806 shaker at 120 rpm for 30 min. Cells were filtered through a 100 µm filter, lysed with ACK lysing
807 buffer (Gibco), and resuspended as single cell suspensions for downstream analysis. All flow
808 cytometry analyses of tumor-bearing lungs were performed on live $CD45\text{-}PECy7^-$ cells. For bulk
809 RNAseq and single cell RNAseq experiments, lung single cell suspensions were cryopreserved
810 in complete RPMI supplemented with 10% FBS and 10% DMSO.
811
812 *Flow Cytometry*

813 Cells were stained using the Live/Dead Fixable Aqua Dead Cell stain kit (Invitrogen) according to
814 the manufacturer's protocol. For surface staining, cells were incubated at 4°C for 30 min in
815 staining buffer (PBS, 2% FBS) with the following directly conjugated antibodies for murine proteins
816 (from BioLegend unless otherwise specified): anti-CD4 (RM4-5), -CD8 (53-6.7), -CD45.1 (A20), -
817 CD45.2 (104), -CD45 (30-F11), -CD3 (145-2C11), -CD19 (eBio1D3, Thermo Fisher), -PD-1
818 (29F.1A12), -LAG-3 (C9B7W), -TIM3 (RMT3-23), -Tox (REA473, Miltenyi), -Thy1.1 (OX-7),
819 Thy1.2 (53-2.1), -B220 (RA3-6B2), NKp46 (29A1.4), NK1.1 (PK136), -CD11b (M1/70), -CD11c
820 (N418), -Ly6C (HK1.4, Thermo Fisher), -Ly6G (1A8), -F4/80 (BM8), I-A/I-E (M5/114.15.2, Thermo
821 Fisher), -CD24 (M1/69), -CD64 (X54-5/7.1), -SiglecF (E50-2440, BD Biosciences), -PD-L1
822 (10F.9G2), -EpCAM (G8.8, Thermo Fisher); or with the following directly conjugated antibodies
823 for human proteins: anti-ROR1 (2A2, Miltenyi Biotec). Recombinant Fc-hROR1 (Fred Hutchinson
824 Cancer Center Protein Core) and anti-human IgG secondary antibody (HP6017, BioLegend) was
825 used to measure ROR1 CAR expression. For intracellular staining, cells were surface stained as
826 described, washed and permeabilized for 20 min with eBioscience Fix/Perm kit at 4°C. Cells were
827 stained for 30 min at 4°C in 1X Perm/Wash buffer (eBioscience) with anti-mouse IFN-γ (XMG1;
828 Thermo Fisher), -TNFα (MP6XT22, Thermo Fisher), -IL-2 (JES6-5H4), -Foxp3 (FJK-16S), -Ki67
829 (B56, BD Biosciences), -Tcf1 (C63D9, Cell Signaling), and/or -cJun (60A8, Cell Signaling). For
830 intracellular cytokine staining following restimulation, cells were stimulated with 50ng/ml PMA and
831 1 µg/ml ionomycin in 0.2 ml complete RPMI in 96-well U-bottomed plates (Costar) at 37°C, 5%
832 CO_2 for 6 hr. GolgiPlug (BD Biosciences) was added to all wells according to the manufacturer's
833 protocol at the beginning of co-culture. All data were acquired on FACS Symphony or Canto II
834 flow cytometers (BD Biosciences) and analyzed using FlowJo software (Treestar).
835
836 *In Vitro Proliferation Assay*
837 For analysis of CAR-T cell proliferation *in vitro*, cells were incubated with 10 uM Cell Trace Blue
838 (Thermo Fisher) in PBS for 9 mins at 37°C and washed with 100% FBS. Cell Trace Blue-labeled
839 T cells were stimulated with 50ng/ml PMA and 1 µg/ml ionomycin in 0.2 ml complete RPMI in 96-
840 well U-bottomed plates (Costar) at 37°C, 5% CO_2 for 72 hr and analyzed by flow cytometry.
841 Proliferation index was calculated from Cell Trace Blue dye dilution profiles using FlowJo software
842 (Tree Star).
843
844 *Immunohistochemistry*
845 Lungs were fixed in 10% neutral-buffered formalin. Formalin-fixed paraffin-embedded tissues
846 were sectioned at 4 microns onto positively-charged slides and baked for 1 hr at 60°C. The slides

847 were then dewaxed and stained on a Leica BOND Rx autostainer (Leica, Buffalo Grove, IL) using
848 Leica Bond reagents for dewaxing (Dewax Solution). Antigen retrieval was performed at 100°C
849 for 20 min using Leica Epitope Retrieval Solution 1 (Leica AR9961). Endogenous peroxidase was
850 blocked with H2O2 (in the Leica kit D59800) for 5 min followed by protein blocking with TCT buffer
851 (0.05 M Tris, 0.15 M NaCl, 0.25% Casein, 0.1% Tween 20, pH 7.6 +/- 0.1) for 10 min. Primary
852 rabbit anti-ROR1 antibody at 1:500 (Cell Signaling #16540) or rabbit anti-CD8 antibody at 1:200
853 (Cell Signaling #98941) was applied for 60 minutes followed by the Refine reagent Rbt-HRP
854 polymer (in the Leica kit D59800) for 12 minutes. Staining was visualized using Mixed Refine
855 DAB (in the Leica kit D59800) and then counter-stained with Hematoxylin (in the Leica kit D59800)
856 for 4 minutes, rinsed and dehydrated and then cover-slipped. Percent ROR1$^+$ cells and CD8$^+$
857 localization within tumors was quantified using HALO software (Indica Labs).
858
859 *Single-Cell RNA Sequencing*
860 Cryopreserved lung tumor cell suspensions and CAR-T infusion products were thawed,
861 washed, and labeled with TotalSeq-C anti-mouse Hashtags (Biolegend) according to the
862 manufacturer's protocol. Following hashing, equal numbers of live cells were pooled from 3 mice
863 in each treatment group to form 4 pools: D9 ROR1 CAR, D9 cJun.ROR1 CAR, D30 ROR1 CAR,
864 D30 cJun.ROR1 CAR. For analysis of T cells, CD8$^+$ T cells were isolated from each pool using
865 the Mouse CD8a Positive Selection Kit II (Stem Cell). For analysis of the TME, each pool was
866 stained Live/Dead Fixable Aqua Dead Cell stain kit (Invitrogen) and live CD45-PECy7$^-$ cells were
867 sorted. For analysis of CAR-T infusion products, CAR-T cells were used directly after hashing.
868 Libraries from CAR-T infusion product, T cell, and TME samples were prepared using the 10X
869 Genomics Chromium GEM-X Single Cell 5' Kit as per the manufacturer's instructions and were
870 sequenced on an Illumina NextSeq 2000 according to the standard 10X Genomics protocol.
871 Resulting reads were aligned to modified reference genome which includes sequences
872 for the ROR1 scFv, tCd19-GFP, and cJun transgenes, using CellRanger (v.8.0.0) software from
873 10X Genomics. HDF5 matrix files were imported into R using the Seurat v5 package. Cells whose
874 UMI counts for mitochondrial genes greater than 10% were excluded from downstream analysis.
875 Cells with between 200 and 7000 genes expressed per cell were included in the analysis. Hashtag
876 oligos (HTO) assay was demultiplexed using Seurat function, HTODemux, to assign hashes and
877 identify cells with more than one hash to be excluded. Scrublet was used to identify potential
878 multiplets which were excluded from downstream analysis. We obtained the following total
879 numbers of cells for each sample after filtering cells for quality: 25458 cells (T cells) and 39639
880 cells (TME).

881

882 *Clustering, Differential Expression, Geneset Scores, and Differential Abundance Analysis*

883 Clustering was performed using Seurat on CAR+ cell clusters in the T cells population,
884 numbering 8766 cells. For unsupervised clustering of cell expression profiles, expression matrices
885 were first normalized using SCTransform, while regressing out mitochondrial percentage. We
886 then performed PCA dimension reduction, followed by FindNeighbors, FindClusters with
887 resolution of 0.8, and UMAP reduction on the first 10 dimensions. Cell annotation was done using
888 cluster markers from FindAllMarkers on upregulated genes using the following settings: log fold
889 change threshold of 0.25, p-adjusted threshold of 0.05, and genes expressed in at least 10% of
890 the cluster (mitochondrial and ribosomal genes were not included in input features). Relative
891 expression of specific gene sets across cells were calculated using AddModuleScore function.

892 Differential abundance analysis was performed using miloR package (v 2.0.0) to identify
893 enrichment of either treatment group (ROR1 CAR-T versus cJun.ROR1 CAR-T). K-nearest
894 neighbor (k-NN) graph was constructed using miloR standard workflow, using k = 30 and prop =
895 0.5 to define neighborhoods. We included "sample_hash" variable as covariate to account for
896 variation across different mouse IDs and time points. Enrichment was assessed using Spatial
897 false discovery rate (SpatialFDR) threshold of < 0.05. Each neighborhood was annotated based
898 on the predominant cell type, with those containing less than 70% of a single cell type labeled as
899 "Mixed" neighborhoods. We used a set of 1000 highly variable genes, identified with
900 modelGeneVar() and getTopHVGs() from scran R package (v.1.32.0), as input features for
901 differential gene expression analysis between all neighborhoods enriched in ROR1 CAR-T versus
902 cJun.ROR1 CAR-T. Neighborhood expression profiles were aggregated by treatment group, and
903 significant markers were identified using adjusted p-value < 0.05.

904

905 *Xenium Custom Probe Panel Design and In Situ Gene Expression*

906 A 100 gene custom add on *in situ* gene expression panel was generated with the Xenium
907 Panel Designer Tool by 10x Genomics (online tool). The custom design was informed by
908 annotated 5' single-cell RNA sequencing data described in this study (Fig.3C) and included
909 custom probes for the ROR1-Cre (*SS109-CRtumor*) and ROR1 CAR (*ROR1_CAR*-T) transgenes,
910 to enable detection of ROR1^{+} tumor and CAR^{+} T cells. Probes for 99 genes identified as
911 differentially expressed and biologically informative from the combined dataset were developed
912 to augment the Xenium Mouse Tissue Atlasing Panel, which includes 379 genes for identifying
913 major mouse cell types. Throughout the panel design process, we prioritized probe coverage for
914 key cell types of interest, ensuring robust representation for populations such as macrophages,

915 B cells, dendritic cells, fibroblasts, neutrophils, NK cells, various T cell subsets (including Th17
916 and Treg), and multiple tumor/stroma subpopulations. Probe selection was optimized to maximize
917 detection sensitivity across these cell types while carefully managing allocation of the detection
918 budget to minimize optical crowding. Each gene's probe sets were chosen to balance coverage
919 and specificity, accommodating the biological heterogeneity of the sample.
920 Formalin-fixed paraffin embedded (FFPE) tissue blocks were sectioned and placed on the
921 Xenium slides as outlined in the 10X Genomics Xenium In Situ Protocols FFPE Tissue
922 Preparation Guide CG000578 Rev. C. Slides were incubated in a covered container in the
923 Eppendorf Innova at 42°C for 3 hr to further adhere the tissue sections to the slide. Slides were
924 then stored in a desiccator at room temperature in the dark until ready to
925 proceed. Deparaffinization and decrosslinking were performed per the 10X Genomics
926 CG000580-Rev C protocol. Briefly, slides were incubated in a covered container in the Eppendorf
927 Innova at 60°C for 2 hr. After cooling to room temperature, the tissue sections underwent a series
928 of submersions in xylene, ethanol, and nuclease free water to complete the deparaffinization
929 process. The slides were loaded into the provided Xenium cassettes, a decrosslinking buffer
930 added, and the slides incubated on the thermocycler adapter to decrosslink and permeabilize the
931 sections. Xenium In Situ Gene Expression User Guide (CG000584 Rev. F) was followed for
932 subsequent steps as follows. Probe preparation was performed by heating the Mouse Multi-
933 Tissue panel + custom add on (described above) to 95°C for 2 min before snap cooling on ice for
934 1 min. The mix of probes and buffer was added to the slides and incubated overnight for a
935 minimum of 16 hr at 50°C. Slides were washed with PBS-T and incubated with a post hybridization
936 wash buffer for 30 min at 37°C. The padlock probes were then ligated at the junction by incubating
937 with a ligase enzyme for 2 hr at 37°C. Following ligation and washing with PBS-T, rolling circle
938 amplification was performed for 2 hr at 30°C\ to amplify the signal from each probe. Slides were
939 prepared for imaging by applying an autofluorescence quenching solution followed by nuclei
940 staining before loading on to the Xenium instrument as instructed by Xenium Analyzer User Guide
941 (CG000584 Rev. E). Upon completion of the run, slides underwent H&E staining following
942 quencher removal in a 10 mM sodium hydrosulfite solution for 10 min. Staining was performed
943 according to Xenium In Situ Gene Expression-Post-Xenium Analyzer H&E staining demonstrated
944 protocol (CG000613 Rev. B).
945
946 *Xenium Analysis*
947 Raw Xenium spatial transcriptomic data was segmented using the Proseg algorithm.[136] All
948 subsequent data processing and analysis was performed in Python using the scanpy v1.9.8[137]

949 and squidpy v1.5.0[138] packages. For each sample, low quality cells with fewer than 10 total
950 transcripts were removed, and genes detected in fewer than 5 cells were removed. Transcriptional
951 data was then log-normalized and PCA-transformed. A nearest-neighbor graph was constructed
952 and used to generate UMAP representation and Leiden clusters. CAR-T cell clusters were
953 identified based on expression of the *ROR1_CAR-T* marker. Those CAR-T cells were then
954 separately subclustered: a nearest-neighbors graph was constructed based on expression of only
955 T cell marker genes (*Tcf7, Mki67, Pdcd1, Havcr2, Ifng, Gzmb, Prdm1, Tox, Foxp3, Entpd1*) for
956 identification of relevant T cell subsets, which was then used for generation of a UMAP and Leiden
957 subclusters.
958 To identify spatial regions (tumor, airway/blood vessel, and normal lung parenchyma), an
959 additional nearest-neighbor graph was constructed based on spatial coordinates of cells. A joint
960 graph was constructed from the two nearest-neighbor graphs (the one constructed from spatial
961 coordinates as well as the graph constructed from gene expression), with the spatial coordinate
962 graph weighted at between 0.5 and 0.6, depending on the sample. Leiden clustering was then
963 performed using this joint graph, with resolution 0.7. Resulting spatial clusters were combined in
964 some cases, using the H&E image as a reference. To identify individual tumors, Leiden clustering
965 based on only the spatial coordinate nearest-neighbor graph was performed on the cells identified
966 as belonging to tumor regions. Clusters were again combined when necessary, according to the
967 H&E image. Abundance analysis was performed by calculating the relative proportion of each
968 cluster of interest out of the total number of cells in the region of interest (individual tumors or
969 entire non-tumor region). Proximity analysis was performed using the co-occurrence and
970 neighborhood enrichment functions in squidpy.
971
972 **QUANTIFICATION AND STATISTICAL ANALYSIS**
973 All data are presented as the mean values ± SEM. Statistical significance was determined by one-
974 way ANOVA with Tukey's post-test, two-way ANOVA with Tukey's post-test, log-rank Mantel-Cox
975 test, unpaired Student's two-way t-test, or paired Student's two-way t-test as indicated in figure
976 legends using Prism software (Graphpad). Statistical significance was established at the levels of
977 *, $p<0.05$; **, $p<0.005$; ***, $p<0.0005$; ****, $p<0.0001$.
978
979 **List of Supplementary Materials**
980 Fig. S1 to S6.

981 **References**

982 1 Siegel, R., Ma, J., Zou, Z. & Jemal, A. Cancer statistics, 2014. *CA: a cancer journal for*
983 *clinicians* **64**, 9 - 29 (2014). https://doi.org/10.3322/caac.21208
984 2 Johnson, D. B., Rioth, M. J. & Horn, L. Immune checkpoint inhibitors in NSCLC. *Curr Treat*
985 *Options Oncol* **15**, 658-669 (2014). https://doi.org/10.1007/s11864-014-0305-5
986 3 Porter, D. L. *et al.* Chimeric antigen receptor T cells persist and induce sustained
987 remissions in relapsed refractory chronic lymphocytic leukemia. *Sci Transl Med* **7**,
988 303ra139 (2015). https://doi.org/10.1126/scitranslmed.aac5415
989 4 Porter, D. L., Levine, B. L., Kalos, M., Bagg, A. & June, C. H. Chimeric antigen receptor-
990 modified T cells in chronic lymphoid leukemia. *The New England journal of medicine* **365**,
991 725 - 733 (2011). https://doi.org/10.1056/nejmoa1103849
992 5 Brentjens, R. J. *et al.* CD19-targeted T cells rapidly induce molecular remissions in adults
993 with chemotherapy-refractory acute lymphoblastic leukemia. *Science translational*
994 *medicine* **5**, 177ra138 - 177ra138 (2013). https://doi.org/10.1126/scitranslmed.3005930
995 6 Brentjens, R. J. *et al.* Safety and persistence of adoptively transferred autologous CD19-
996 targeted T cells in patients with relapsed or chemotherapy refractory B-cell leukemias.
997 *Blood* **118**, 4817 - 4828 (2011). https://doi.org/10.1182/blood-2011-04-348540
998 7 Kalos, M. *et al.* T cells with chimeric antigen receptors have potent antitumor effects and
999 can establish memory in patients with advanced leukemia. *Science translational medicine*
1000 **3**, 95ra73 - 95ra73 (2011). https://doi.org/10.1126/scitranslmed.3002842
1001 8 Mullard, A. Second anticancer CAR T therapy receives FDA approval. *Nat Rev Drug*
1002 *Discov* **16**, 818 (2017). https://doi.org/10.1038/nrd.2017.249
1003 9 Mullard, A. FDA approves first CAR T therapy. *Nat Rev Drug Discov* **16**, 669 (2017).
1004 https://doi.org/10.1038/nrd.2017.196
1005 10 Melenhorst, J. J. *et al.* Decade-long leukaemia remissions with persistence of CD4(+) CAR
1006 T cells. *Nature* (2022). https://doi.org/10.1038/s41586-021-04390-6
1007 11 Scholler, J. *et al.* Decade-long safety and function of retroviral-modified chimeric antigen
1008 receptor T cells. *Sci Transl Med* **4**, 132ra153 (2012).
1009 https://doi.org/10.1126/scitranslmed.3003761
1010 12 Turtle, C. J. *et al.* Immunotherapy of non-Hodgkin's lymphoma with a defined ratio of CD8+
1011 and CD4+ CD19-specific chimeric antigen receptor-modified T cells. *Science translational*
1012 *medicine* **8**, 355ra116 - 355ra116 (2016). https://doi.org/10.1126/scitranslmed.aaf8621

1013 13 Srivastava, S. & Riddell, S. R. Chimeric Antigen Receptor T Cell Therapy: Challenges to
1014 Bench-to-Bedside Efficacy. *Journal of immunology (Baltimore, Md. : 1950)* **200**, 459 - 468
1015 (2018). https://doi.org/10.4049/jimmunol.1701155
1016 14 June, C. H. & Sadelain, M. Chimeric Antigen Receptor Therapy. *N Engl J Med* **379**, 64-73
1017 (2018). https://doi.org/10.1056/NEJMra1706169
1018 15 Brown, C. E. & Mackall, C. L. CAR T cell therapy: inroads to response and resistance.
1019 *Nature reviews. Immunology* **19**, 73 - 74 (2019). https://doi.org/10.1038/s41577-018-
1020 0119-y
1021 16 D'Aloia, M. M., Zizzari, I. G., Sacchetti, B., Pierelli, L. & Alimandi, M. CAR-T cells: the long
1022 and winding road to solid tumors. *Cell Death Dis* **9**, 282 (2018).
1023 https://doi.org/10.1038/s41419-018-0278-6
1024 17 Newick, K., Moon, E. & Albelda, S. M. Chimeric antigen receptor T-cell therapy for solid
1025 tumors. *Molecular therapy oncolytics* **3**, 16006 (2016). https://doi.org/10.1038/mto.2016.6
1026 18 Schmidts, A. & Maus, M. V. Making CAR T Cells a Solid Option for Solid Tumors. *Front*
1027 *Immunol* **9**, 2593 (2018). https://doi.org/10.3389/fimmu.2018.02593
1028 19 Balakrishnan, A. *et al.* Analysis of ROR1 Protein Expression in Human Cancer and Normal
1029 Tissues. *Clinical cancer research : an official journal of the American Association for*
1030 *Cancer Research* **23**, 3061 - 3071 (2017). https://doi.org/10.1158/1078-0432.ccr-16-2083
1031 20 Berger, C. *et al.* Safety of targeting ROR1 in primates with chimeric antigen receptor-
1032 modified T cells. *Cancer immunology research* **3**, 206 - 216 (2015).
1033 https://doi.org/10.1158/2326-6066.cir-14-0163
1034 21 Srivastava, S. *et al.* Immunogenic Chemotherapy Enhances Recruitment of CAR-T Cells
1035 to Lung Tumors and Improves Antitumor Efficacy when Combined with Checkpoint
1036 Blockade. *Cancer Cell* **39**, 193-208 e110 (2021).
1037 https://doi.org/10.1016/j.ccell.2020.11.005
1038 22 Srivastava, S. *et al.* Logic-Gated ROR1 Chimeric Antigen Receptor Expression Rescues
1039 T Cell-Mediated Toxicity to Normal Tissues and Enables Selective Tumor Targeting.
1040 *Cancer cell* **35**, 489 - 503.e488 (2019). https://doi.org/10.1016/j.ccell.2019.02.003
1041 23 Jaeger-Ruckstuhl, C. A. *et al.* Phase 1 Study of ROR1 Specific CAR T Cells in Advanced
1042 Hematopoietic and Epithelial Malignancies. *Clin Cancer Res* (2024).
1043 https://doi.org/10.1158/1078-0432.CCR-24-2172
1044 24 Grosser, R., Cherkassky, L., Chintala, N. & Adusumilli, P. S. Combination Immunotherapy
1045 with CAR T Cells and Checkpoint Blockade for the Treatment of Solid Tumors. *Cancer*
1046 *Cell* **36**, 471-482 (2019). https://doi.org/10.1016/j.ccell.2019.09.006

1047 25 Pérez-Moreno, M. A. *et al.* Combined or Sequential Treatment with Immune Checkpoint
1048 Inhibitors and Car-T Cell Therapies for the Management of Haematological Malignancies:
1049 A Systematic Review. *Int J Mol Sci* **24** (2023). https://doi.org/10.3390/ijms241914780
1050 26 Li, A. M. *et al.* Checkpoint Inhibitors Augment CD19-Directed Chimeric Antigen Receptor
1051 (CAR) T Cell Therapy in Relapsed B-Cell Acute Lymphoblastic Leukemia. *Blood* **132**, 556-
1052 556 (2018). https://doi.org/10.1182/blood-2018-99-112572
1053 27 Maude, S. L. *et al.* (American Society of Clinical Oncology, 2017).
1054 28 Cao, Y. *et al.* Anti-CD19 Chimeric Antigen Receptor T Cells in Combination With
1055 Nivolumab Are Safe and Effective Against Relapsed/Refractory B-Cell Non-hodgkin
1056 Lymphoma. *Front Oncol* **9**, 767 (2019). https://doi.org/10.3389/fonc.2019.00767
1057 29 Siddiqi, T. *et al.* Safety of lisocabtagene maraleucel given with Durvalumab in patients
1058 with relapsed/refractory aggressive B-cell non Hodgkin lymphoma: first results from the
1059 platform study. *Hematological Oncology* **37**, 171-172 (2019).
1060 30 Jacobson, C. A. *et al.* Abstract CT055: Phase 1/2 primary analysis of ZUMA-6:
1061 Axicabtagene ciloleucel (Axi-Cel) in combination With atezolizumab (Atezo) for the
1062 treatment of patients (Pts) with refractory diffuse large B cell lymphoma (DLBCL). *Cancer*
1063 *Research* **80**, CT055-CT055 (2020).
1064 31 Osborne, W. *et al.* (American Society of Clinical Oncology, 2020).
1065 32 Chong, E. A. *et al.* Pembrolizumab for B-cell lymphomas relapsing after or refractory to
1066 CD19-directed CAR T-cell therapy. *Blood, The Journal of the American Society of*
1067 *Hematology* **139**, 1026-1038 (2022).
1068 33 Vinaud Hirayama, A. *et al.* Timing of PD-L1 blockade with durvalumab may affect
1069 outcomes of CD19 CAR-T cell therapy for relapsed/Refractory large B-Cell lymphoma.
1070 *Blood* **140**, 7447-7449 (2022).
1071 34 Jaeger, U. *et al.* Safety and efficacy of tisagenlecleucel plus pembrolizumab in patients
1072 with r/r DLBCL: phase 1b PORTIA study results. *Blood Advances* **7**, 2283-2286 (2023).
1073 35 Beltra, J. C. *et al.* Developmental Relationships of Four Exhausted CD8(+) T Cell Subsets
1074 Reveals Underlying Transcriptional and Epigenetic Landscape Control Mechanisms.
1075 *Immunity* **52**, 825-841 e828 (2020). https://doi.org/10.1016/j.immuni.2020.04.014
1076 36 Im, S. J. *et al.* Defining CD8+ T cells that provide the proliferative burst after PD-1 therapy.
1077 *Nature* **537**, 417-421 (2016). https://doi.org/10.1038/nature19330
1078 37 Jadhav, R. R. *et al.* Epigenetic signature of PD-1+ TCF1+ CD8 T cells that act as resource
1079 cells during chronic viral infection and respond to PD-1 blockade. *Proc National Acad Sci*
1080 **116**, 14113-14118 (2019). https://doi.org/10.1073/pnas.1903520116 PMID - 31227606

1081 38 Siddiqui, I. *et al.* Intratumoral Tcf1(+)PD-1(+)CD8(+) T Cells with Stem-like Properties
1082 Promote Tumor Control in Response to Vaccination and Checkpoint Blockade
1083 Immunotherapy. *Immunity* **50**, 195-211 e110 (2019).
1084 https://doi.org/10.1016/j.immuni.2018.12.021
1085 39 Kallies, A., Zehn, D. & Utzschneider, D. T. Precursor exhausted T cells: key to successful
1086 immunotherapy? *Nat Rev Immunol* **20**, 128-136 (2020). https://doi.org/10.1038/s41577-
1087 019-0223-7
1088 40 Utzschneider, D. T. *et al.* T Cell Factor 1-Expressing Memory-like CD8(+) T Cells Sustain
1089 the Immune Response to Chronic Viral Infections. *Immunity* **45**, 415-427 (2016).
1090 https://doi.org/10.1016/j.immuni.2016.07.021
1091 41 Utzschneider, D. T. *et al.* Early precursor T cells establish and propagate T cell exhaustion
1092 in chronic infection. *Nat Immunol* **21**, 1256-1266 (2020). https://doi.org/10.1038/s41590-
1093 020-0760-z
1094 42 He, R. *et al.* Follicular CXCR5- expressing CD8(+) T cells curtail chronic viral infection.
1095 *Nature* **537**, 412-428 (2016). https://doi.org/10.1038/nature19317
1096 43 Miller, B. C. *et al.* Subsets of exhausted CD8+ T cells differentially mediate tumor control
1097 and respond to checkpoint blockade. *Nature immunology* **20**, 326 - 336 (2019).
1098 https://doi.org/10.1038/s41590-019-0312-6
1099 44 Blank, C. U. *et al.* Defining 'T cell exhaustion'. *Nat Rev Immunol* **19**, 665-674 (2019).
1100 https://doi.org/10.1038/s41577-019-0221-9
1101 45 Martinez, G. J. *et al.* The transcription factor NFAT promotes exhaustion of activated
1102 CD8(+) T cells. *Immunity* **42**, 265-278 (2015).
1103 https://doi.org/10.1016/j.immuni.2015.01.006
1104 46 Pauken, K. E. & Wherry, E. J. Overcoming T cell exhaustion in infection and cancer.
1105 *Trends in immunology* **36**, 265 - 276 (2015). https://doi.org/10.1016/j.it.2015.02.008
1106 47 Schietinger, A. *et al.* Tumor-Specific T Cell Dysfunction Is a Dynamic Antigen-Driven
1107 Differentiation Program Initiated Early during Tumorigenesis. *Immunity* **45**, 389 - 401
1108 (2016). https://doi.org/10.1016/j.immuni.2016.07.011
1109 48 Wherry, E. J. T cell exhaustion. *Nature Immunology* **12**, 492 (2011).
1110 https://doi.org/10.1038/ni.2035 PMID - 21739672
1111 49 Wherry, E. J. & Kurachi, M. Molecular and cellular insights into T cell exhaustion. *Nat Rev*
1112 *Immunol* **15**, 486-499 (2015). https://doi.org/10.1038/nri3862

1113 50 Gabriel, S. S. *et al.* Transforming growth factor-beta-regulated mTOR activity preserves
1114 cellular metabolism to maintain long-term T cell responses in chronic infection. *Immunity*
1115 **54**, 1698-1714 e1695 (2021). https://doi.org/10.1016/j.immuni.2021.06.007
1116 51 Schenkel, J. M. *et al.* Conventional type I dendritic cells maintain a reservoir of proliferative
1117 tumor-antigen specific TCF-1(+) CD8(+) T cells in tumor-draining lymph nodes. *Immunity*
1118 **54**, 2338-2353 e2336 (2021). https://doi.org/10.1016/j.immuni.2021.08.026
1119 52 Connolly, K. A. *et al.* A reservoir of stem-like CD8(+) T cells in the tumor-draining lymph
1120 node preserves the ongoing antitumor immune response. *Sci Immunol* **6**, eabg7836
1121 (2021). https://doi.org/10.1126/sciimmunol.abg7836
1122 53 Jansen, C. S. *et al.* An intra-tumoral niche maintains and differentiates stem-like CD8 T
1123 cells. *Nature* **576**, 465-470 (2019). https://doi.org/10.1038/s41586-019-1836-5
1124 54 Stoltzfus, C. R. *et al.* Multi-Parameter Quantitative Imaging of Tumor Microenvironments
1125 Reveals Perivascular Immune Niches Associated With Anti-Tumor Immunity. *Front*
1126 *Immunol* **12**, 726492 (2021). https://doi.org/10.3389/fimmu.2021.726492
1127 55 Eberhardt, C. S. *et al.* Functional HPV-specific PD-1(+) stem-like CD8 T cells in head and
1128 neck cancer. *Nature* **597**, 279-284 (2021). https://doi.org/10.1038/s41586-021-03862-z
1129 56 Prokhnevska, N. a. C., Maria A. and Valanparambil, Rajesh M. and Sobierajska, Ewelina
1130 and Barwick, Benjamin G. and Jansen, Caroline S. and Moon, Adriana R. and Gregorova,
1131 Petra and delBalzo, Luke and Greenwald, Rachel and Bilen, Mehmet A. and Alemozaffar,
1132 Mehrdad and Cimmino, Cara and Larsen, Christian and Master, Viraj A. and Sanda, Martin
1133 and Kissick, Haydn. CD8 T Cell Activation in Cancer is Comprised of Two Distinct Phases.
1134 *Immunity* (2021). https://doi.org/http://dx.doi.org/10.2139/ssrn.3893902
1135 57 Dahling, S. *et al.* Type 1 conventional dendritic cells maintain and guide the differentiation
1136 of precursors of exhausted T cells in distinct cellular niches. *Immunity* **55**, 656-670 e658
1137 (2022). https://doi.org/10.1016/j.immuni.2022.03.006
1138 58 Gearty, S. V. *et al.* An autoimmune stem-like CD8 T cell population drives type 1 diabetes.
1139 *Nature* (2021). https://doi.org/10.1038/s41586-021-04248-x
1140 59 Hudson, W. H. *et al.* Proliferating Transitory T Cells with an Effector-like Transcriptional
1141 Signature Emerge from PD-1(+) Stem-like CD8(+) T Cells during Chronic Infection.
1142 *Immunity* **51**, 1043-1058 e1044 (2019). https://doi.org/10.1016/j.immuni.2019.11.002
1143 60 Scharping, N. E. *et al.* Mitochondrial stress induced by continuous stimulation under
1144 hypoxia rapidly drives T cell exhaustion. *Nat Immunol* **22**, 205-215 (2021).
1145 https://doi.org/10.1038/s41590-020-00834-9

1146 61 Dhatchinamoorthy, K., Colbert, J. D. & Rock, K. L. Cancer Immune Evasion Through Loss
1147 of MHC Class I Antigen Presentation. *Front Immunol* **12**, 636568 (2021).
1148 https://doi.org/10.3389/fimmu.2021.636568
1149 62 DuPage, M., Dooley, A. L. & Jacks, T. Conditional mouse lung cancer models using
1150 adenoviral or lentiviral delivery of Cre recombinase. *Nature protocols* **4**, 1064 - 1072
1151 (2009). https://doi.org/10.1038/nprot.2009.95
1152 63 DuPage, M. *et al.* Endogenous T cell responses to antigens expressed in lung
1153 adenocarcinomas delay malignant tumor progression. *Cancer cell* **19**, 72 - 85 (2011).
1154 https://doi.org/10.1016/j.ccr.2010.11.011
1155 64 DuPage, M. & Jacks, T. Genetically engineered mouse models of cancer reveal new
1156 insights about the antitumor immune response. *Current opinion in immunology* **25**, 192 -
1157 199 (2013). https://doi.org/10.1016/j.coi.2013.02.005
1158 65 Lynn, R. C. *et al.* c-Jun overexpression in CAR T cells induces exhaustion resistance.
1159 *Nature* **576**, 293-300 (2019). https://doi.org/10.1038/s41586-019-1805-z PMID -
1160 31802004
1161 66 Seo, H. *et al.* BATF and IRF4 cooperate to counter exhaustion in tumor-infiltrating CAR T
1162 cells. *Nature Immunology* **22**, 983-995 (2021). https://doi.org/10.1038/s41590-021-00964-
1163 8
1164 67 Liu, Z. *et al.* Systematic comparison of 2A peptides for cloning multi-genes in a
1165 polycistronic vector. *Sci Rep* **7**, 2193 (2017). https://doi.org/10.1038/s41598-017-02460-2
1166 68 Cabrera, A. *et al.* The sound of silence: Transgene silencing in mammalian cell
1167 engineering. *Cell Syst* **13**, 950-973 (2022). https://doi.org/10.1016/j.cels.2022.11.005
1168 69 Hudecek, M. *et al.* Receptor affinity and extracellular domain modifications affect tumor
1169 recognition by ROR1-specific chimeric antigen receptor T cells. *Clinical cancer research :*
1170 *an official journal of the American Association for Cancer Research* **19**, 3153-3164 (2013).
1171 https://doi.org/10.1158/1078-0432.CCR-13-0330
1172 70 Yang, J. *et al.* Therapeutic potential and challenges of targeting receptor tyrosine kinase
1173 ROR1 with monoclonal antibodies in B-cell malignancies. *PLoS One* **6**, e21018 (2011).
1174 https://doi.org/10.1371/journal.pone.0021018
1175 71 Gattinoni, L. *et al.* Acquisition of full effector function in vitro paradoxically impairs the in
1176 vivo antitumor efficacy of adoptively transferred CD8+ T cells. *J Clin Invest* **115**, 1616-
1177 1626 (2005). https://doi.org/10.1172/JCI24480
1178 72 Gattinoni, L., Klebanoff, C. A. & Restifo, N. P. Paths to stemness: building the ultimate
1179 antitumour T cell. *Nat Rev Cancer* **12**, 671-684 (2012). https://doi.org/10.1038/nrc3322

1180 73 Klebanoff, C. A. *et al.* Central memory self/tumor-reactive CD8+ T cells confer superior
1181 antitumor immunity compared with effector memory T cells. *Proc Natl Acad Sci U S A* **102**,
1182 9571-9576 (2005). https://doi.org/10.1073/pnas.0503726102
1183 74 Xu, Y. *et al.* Closely related T-memory stem cells correlate with in vivo expansion of
1184 CAR.CD19-T cells and are preserved by IL-7 and IL-15. *Blood* **123**, 3750-3759 (2014).
1185 https://doi.org/10.1182/blood-2014-01-552174
1186 75 Louis, C. U. *et al.* Antitumor activity and long-term fate of chimeric antigen receptor-
1187 positive T cells in patients with neuroblastoma. *Blood* **118**, 6050-6056 (2011).
1188 https://doi.org/10.1182/blood-2011-05-354449
1189 76 Monfrini, C. *et al.* Phenotypic Composition of Commercial Anti-CD19 CAR T Cells Affects
1190 In Vivo Expansion and Disease Response in Patients with Large B-cell Lymphoma. *Clin*
1191 *Cancer Res* **28**, 3378-3386 (2022). https://doi.org/10.1158/1078-0432.Ccr-22-0164
1192 77 Sommermeyer, D. *et al.* Chimeric antigen receptor-modified T cells derived from defined
1193 CD8 and CD4 subsets confer superior antitumor reactivity in vivo. *Leukemia* (2015).
1194 https://doi.org/10.1038/leu.2015.247
1195 78 Miller, B. C. *et al.* Subsets of exhausted CD8(+) T cells differentially mediate tumor control
1196 and respond to checkpoint blockade. *Nat Immunol* **20**, 326-336 (2019).
1197 https://doi.org/10.1038/s41590-019-0312-6
1198 79 Oliveira, G. *et al.* Phenotype, specificity and avidity of antitumour CD8(+) T cells in
1199 melanoma. *Nature* **596**, 119-125 (2021). https://doi.org/10.1038/s41586-021-03704-y
1200 80 Dann, E., Henderson, N. C., Teichmann, S. A., Morgan, M. D. & Marioni, J. C. Differential
1201 abundance testing on single-cell data using k-nearest neighbor graphs. *Nat Biotechnol* **40**,
1202 245-253 (2022). https://doi.org/10.1038/s41587-021-01033-z
1203 81 Weiss, S. A. *et al.* Epigenetic tuning of PD-1 expression improves exhausted T cell
1204 function and viral control. *Nat Immunol* **25**, 1871-1883 (2024).
1205 https://doi.org/10.1038/s41590-024-01961-3
1206 82 Sen, D. R. *et al.* The epigenetic landscape of T cell exhaustion. *Science* **354**, 1165-1169
1207 (2016). https://doi.org/10.1126/science.aae0491
1208 83 Pauken, K. E. *et al.* Epigenetic stability of exhausted T cells limits durability of
1209 reinvigoration by PD-1 blockade. *Science* **354**, 1160-1165 (2016).
1210 https://doi.org/10.1126/science.aaf2807
1211 84 Blackburn, S. D. *et al.* Coregulation of CD8+ T cell exhaustion by multiple inhibitory
1212 receptors during chronic viral infection. *Nat Immunol* **10**, 29-37 (2009).
1213 https://doi.org/10.1038/ni.1679

1214 85 Alfei, F. *et al.* TOX reinforces the phenotype and longevity of exhausted T cells in chronic
1215 viral infection. *Nature* **571**, 265 - 269 (2019). https://doi.org/10.1038/s41586-019-1326-9
1216 86 Khan, O. *et al.* TOX transcriptionally and epigenetically programs CD8+ T cell exhaustion.
1217 *Nature* **571**, 211 - 218 (2019). https://doi.org/10.1038/s41586-019-1325-x
1218 87 Scott, A. C. *et al.* TOX is a critical regulator of tumour-specific T cell differentiation. *Nature*
1219 **571**, 270 - 274 (2019). https://doi.org/10.1038/s41586-019-1324-y
1220 88 Seo, H. *et al.* TOX and TOX2 transcription factors cooperate with NR4A transcription
1221 factors to impose CD8+ T cell exhaustion. *Proceedings of the National Academy of*
1222 *Sciences of the United States of America* **116**, 12410 - 12415 (2019).
1223 https://doi.org/10.1073/pnas.1905675116
1224 89 Nowicki, T. S. *et al.* Epigenetic Suppression of Transgenic T-cell Receptor Expression via
1225 Gamma-Retroviral Vector Methylation in Adoptive Cell Transfer Therapy. *Cancer Discov*
1226 **10**, 1645-1653 (2020). https://doi.org/10.1158/2159-8290.CD-20-0300
1227 90 Eyquem, J. *et al.* Targeting a CAR to the TRAC locus with CRISPR/Cas9 enhances
1228 tumour rejection. *Nature* **543**, 113-117 (2017). https://doi.org/10.1038/nature21405
1229 91 Papavassiliou, A. G. & Musti, A. M. The Multifaceted Output of c-Jun Biological Activity:
1230 Focus at the Junction of CD8 T Cell Activation and Exhaustion. *Cells* **9** (2020).
1231 https://doi.org/10.3390/cells9112470
1232 92 Musti, A. M., Treier, M. & Bohmann, D. Reduced ubiquitin-dependent degradation of c-
1233 Jun after phosphorylation by MAP kinases. *Science* **275**, 400-402 (1997).
1234 https://doi.org/10.1126/science.275.5298.400
1235 93 Conze, D. *et al.* c-Jun NH(2)-terminal kinase (JNK)1 and JNK2 have distinct roles in
1236 CD8(+) T cell activation. *J Exp Med* **195**, 811-823 (2002).
1237 https://doi.org/10.1084/jem.20011508
1238 94 Gao, B., Lee, S. M. & Fang, D. The tyrosine kinase c-Abl protects c-Jun from
1239 ubiquitination-mediated degradation in T cells. *J Biol Chem* **281**, 29711-29718 (2006).
1240 https://doi.org/10.1074/jbc.M604596200
1241 95 Zipfel, P. A., Zhang, W., Quiroz, M. & Pendergast, A. M. Requirement for Abl kinases in T
1242 cell receptor signaling. *Curr Biol* **14**, 1222-1231 (2004).
1243 https://doi.org/10.1016/j.cub.2004.07.021
1244 96 Su, B. *et al.* JNK is involved in signal integration during costimulation of T lymphocytes.
1245 *Cell* **77**, 727-736 (1994). https://doi.org/10.1016/0092-8674(94)90056-6

1246 97 Wartewig, T. *et al.* PD-1 instructs a tumor-suppressive metabolic program that restricts
1247 glycolysis and restrains AP-1 activity in T cell lymphoma. *Nat Cancer* **4**, 1508-1525 (2023).
1248 https://doi.org/10.1038/s43018-023-00635-7
1249 98 Zilionis, R. *et al.* Single-Cell Transcriptomics of Human and Mouse Lung Cancers Reveals
1250 Conserved Myeloid Populations across Individuals and Species. *Immunity* **50**, 1317-1334
1251 e1310 (2019). https://doi.org/10.1016/j.immuni.2019.03.009
1252 99 Chen, D. *et al.* Chloroquine modulates antitumor immune response by resetting tumor-
1253 associated macrophages toward M1 phenotype. *Nature Communications* **9**, 873 (2018).
1254 https://doi.org/10.1038/s41467-018-03225-9
1255 100 Ma, Q. *et al.* PlGF signaling and macrophage repolarization contribute to the anti-
1256 neoplastic effect of metformin. *Eur J Pharmacol* **863**, 172696 (2019).
1257 https://doi.org/10.1016/j.ejphar.2019.172696
1258 101 Meng, Y. *et al.* Galactan isolated from Cantharellus cibarius modulates antitumor immune
1259 response by converting tumor-associated macrophages toward M1-like phenotype.
1260 *Carbohydr Polym* **226**, 115295 (2019). https://doi.org/10.1016/j.carbpol.2019.115295
1261 102 Rodell, C. B. *et al.* TLR7/8-agonist-loaded nanoparticles promote the polarization of
1262 tumour-associated macrophages to enhance cancer immunotherapy. *Nature Biomedical*
1263 *Engineering* **2**, 578-588 (2018). https://doi.org/10.1038/s41551-018-0236-8
1264 103 Duan, Z. & Luo, Y. Targeting macrophages in cancer immunotherapy. *Signal Transduction*
1265 *and Targeted Therapy* **6**, 127 (2021). https://doi.org/10.1038/s41392-021-00506-6
1266 104 Sharma, P. *et al.* Immune checkpoint therapy—current perspectives and future directions.
1267 *Cell* **186**, 1652-1669 (2023). https://doi.org/https://doi.org/10.1016/j.cell.2023.03.006
1268 105 Robert, C. A decade of immune-checkpoint inhibitors in cancer therapy. *Nature*
1269 *Communications* **11**, 3801 (2020). https://doi.org/10.1038/s41467-020-17670-y
1270 106 Man, K. *et al.* Transcription Factor IRF4 Promotes CD8(+) T Cell Exhaustion and Limits
1271 the Development of Memory-like T Cells during Chronic Infection. *Immunity* **47**, 1129-
1272 1141.e1125 (2017). https://doi.org/10.1016/j.immuni.2017.11.021
1273 107 Liu, C. *et al.* Neuropilin-1 is a T cell memory checkpoint limiting long-term antitumor
1274 immunity. *Nat Immunol* **21**, 1010-1021 (2020). https://doi.org/10.1038/s41590-020-0733-
1275 2
1276 108 Heitzeneder, S. *et al.* GPC2-CAR T cells tuned for low antigen density mediate potent
1277 activity against neuroblastoma without toxicity. *Cancer Cell* **40**, 53-69.e59 (2022).
1278 https://doi.org/10.1016/j.ccell.2021.12.005

1279 109 Xu, T. *et al.* Coexpression of c-Jun in multiple-chain DAP-CAR-engineered T-cells for solid
1280 tumor therapy. *Immunotherapy* **14**, 1457-1466 (2022). https://doi.org/10.2217/imt-2022-
1281 0171
1282 110 Zuo, S. *et al.* C-JUN overexpressing CAR-T cells in acute myeloid leukemia: preclinical
1283 characterization and phase I trial. *Nature Communications* **15**, 6155 (2024).
1284 https://doi.org/10.1038/s41467-024-50485-9
1285 111 Hussein, M. S., Li, Q., Mao, R., Peng, Y. & He, Y. TCR T cells overexpressing c-Jun have
1286 better functionality with improved tumor infiltration and persistence in hepatocellular
1287 carcinoma. *Front Immunol* **14**, 1114770 (2023).
1288 https://doi.org/10.3389/fimmu.2023.1114770
1289 112 Chan, J. D. *et al.* FOXO1 enhances CAR T cell stemness, metabolic fitness and efficacy.
1290 *Nature* **629**, 201-210 (2024). https://doi.org/10.1038/s41586-024-07242-1
1291 113 Lynn, R. C. *et al.* 285 LYL797 ROR-1 CAR T-cell translational data demonstrated T-cell
1292 reprogramming limited exhaustion, maintained stemness, and resulted in tumor infiltration
1293 and cell killing in patients with solid tumors. *Journal for ImmunoTherapy of Cancer* **12**,
1294 A324 (2024). https://doi.org/10.1136/jitc-2024-SITC2024.0285
1295 114 Kargl, J. *et al.* Neutrophils dominate the immune cell composition in non-small cell lung
1296 cancer. *Nat Commun* **8**, 14381 (2017). https://doi.org/10.1038/ncomms14381
1297 115 Kargl, J. *et al.* Neutrophil content predicts lymphocyte depletion and anti-PD1 treatment
1298 failure in NSCLC. *JCI Insight* **4** (2019). https://doi.org/10.1172/jci.insight.130850
1299 116 Burga, R. A. *et al.* Liver myeloid-derived suppressor cells expand in response to liver
1300 metastases in mice and inhibit the anti-tumor efficacy of anti-CEA CAR-T. *Cancer*
1301 *Immunol Immunother* **64**, 817-829 (2015). https://doi.org/10.1007/s00262-015-1692-6
1302 117 Chocarro, L. *et al.* PD-1/LAG-3 co-signaling profiling uncovers CBL ubiquitin ligases as
1303 key immunotherapy targets. *EMBO Mol Med* **16**, 1791-1816 (2024).
1304 https://doi.org/10.1038/s44321-024-00098-y
1305 118 Liu, R. *et al.* PD-1 signaling negatively regulates the common cytokine receptor gamma
1306 chain via MARCH5-mediated ubiquitination and degradation to suppress anti-tumor
1307 immunity. *Cell Res* **33**, 923-939 (2023). https://doi.org/10.1038/s41422-023-00890-4
1308 119 Kumar, J. *et al.* Deletion of Cbl-b inhibits CD8(+) T-cell exhaustion and promotes CAR T-
1309 cell function. *J Immunother Cancer* **9** (2021). https://doi.org/10.1136/jitc-2020-001688
1310 120 Chien, H.-P. *et al.* Expression of ROR1 has prognostic significance in triple negative
1311 breast cancer. *Virchows Archiv : an international journal of pathology* **468**, 589 - 595
1312 (2016). https://doi.org/10.1007/s00428-016-1911-3

1313 121 Choi, M. Y. *et al.* Phase I Trial: Cirmtuzumab Inhibits ROR1 Signaling and Stemness
1314 Signatures in Patients with Chronic Lymphocytic Leukemia. *Cell stem cell* **22**, 951 -
1315 959.e953 (2018). https://doi.org/10.1016/j.stem.2018.05.018
1316 122 Cui, B. *et al.* High-level ROR1 associates with accelerated disease progression in chronic
1317 lymphocytic leukemia. *Blood* **128**, 2931 - 2940 (2016). https://doi.org/10.1182/blood-2016-
1318 04-712562
1319 123 Henry, C., Hacker, N. & Ford, C. Silencing ROR1 and ROR2 inhibits invasion and
1320 adhesion in an organotypic model of ovarian cancer metastasis. *Oncotarget* **8**, 112727 -
1321 112738 (2017). https://doi.org/10.18632/oncotarget.22559
1322 124 Yamaguchi, T. *et al.* NKX2-1/TITF1/TTF-1-Induced ROR1 is required to sustain EGFR
1323 survival signaling in lung adenocarcinoma. *Cancer cell* **21**, 348 - 361 (2012).
1324 https://doi.org/10.1016/j.ccr.2012.02.008
1325 125 Zhang, H. *et al.* ROR1 expression correlated with poor clinical outcome in human ovarian
1326 cancer. *Scientific reports* **4**, 5811 (2014). https://doi.org/10.1038/srep05811
1327 126 Zhang, S. *et al.* ROR1 is expressed in human breast cancer and associated with enhanced
1328 tumor-cell growth. *PLoS One* **7**, e31127 (2012).
1329 https://doi.org/10.1371/journal.pone.0031127
1330 127 Zheng, Y. Z. *et al.* ROR1 is a novel prognostic biomarker in patients with lung
1331 adenocarcinoma. *Sci Rep* **6**, 36447 (2016). https://doi.org/10.1038/srep36447
1332 128 Zhou, J.-K. *et al.* ROR1 expression as a biomarker for predicting prognosis in patients with
1333 colorectal cancer. *Oncotarget* **8**, 32864 - 32872 (2017).
1334 https://doi.org/10.18632/oncotarget.15860
1335 129 Westcott, P. M. *et al.* The mutational landscapes of genetic and chemical models of Kras-
1336 driven lung cancer. *Nature* **517**, 489-492 (2015). https://doi.org/10.1038/nature13898
1337 130 Koga, T. *et al.* Mapping of genomic EGFRvIII deletions in glioblastoma: insight into
1338 rearrangement mechanisms and biomarker development. *Neuro Oncol* **20**, 1310-1320
1339 (2018). https://doi.org/10.1093/neuonc/noy058
1340 131 Posey, A. D., Jr. *et al.* Engineered CAR T Cells Targeting the Cancer-Associated Tn-
1341 Glycoform of the Membrane Mucin MUC1 Control Adenocarcinoma. *Immunity* **44**, 1444-
1342 1454 (2016). https://doi.org/10.1016/j.immuni.2016.05.014
1343 132 Hudecek, M. *et al.* The B-cell tumor-associated antigen ROR1 can be targeted with T cells
1344 modified to express a ROR1-specific chimeric antigen receptor. *Blood* **116**, 4532-4541
1345 (2010). https://doi.org/10.1182/blood-2010-05-283309

133 Hudecek, M. *et al.* The nonsignaling extracellular spacer domain of chimeric antigen receptors is decisive for in vivo antitumor activity. *Cancer immunology research* **3**, 125 - 135 (2015). https://doi.org/10.1158/2326-6066.cir-14-0127

134 Nguyen, P., Moisini, I. & Geiger, T. L. Identification of a murine CD28 dileucine motif that suppresses single-chain chimeric T-cell receptor expression and function. *Blood* **102**, 4320-4325 (2003). https://doi.org/10.1182/blood-2003-04-1255

135 Yam, P. Y. *et al.* Design of HIV vectors for efficient gene delivery into human hematopoietic cells. *Mol Ther* **5**, 479-484 (2002). https://doi.org/10.1006/mthe.2002.0558

136 Jones, D. C. *et al.* Cell Simulation as Cell Segmentation. *bioRxiv*, 2024.2004.2025.591218 (2024). https://doi.org/10.1101/2024.04.25.591218

137 Wolf, F. A., Angerer, P. & Theis, F. J. SCANPY: large-scale single-cell gene expression data analysis. *Genome Biology* **19**, 15 (2018). https://doi.org/10.1186/s13059-017-1382-0

138 Palla, G. *et al.* Squidpy: a scalable framework for spatial omics analysis. *Nat Methods* **19**, 171-178 (2022). https://doi.org/10.1038/s41592-021-01358-2

Acknowledgements

We wish to thank Ekram Gad, Elena Carlson, and Tracy Goodpaster in Shared Resources and David Sowerby in the Fred Hutch Innovation Lab for technical services, as well as Joshua Veatch, Mark Headley, and Stan Riddell for helpful discussions and reagents. Treatment schematic figures were created with BioRender. This research was also supported by the Preclinical Imaging, Comparative Medicine, and Experimental Histopathology Shared Resources of the Fred Hutch/University of Washington Cancer Consortium.

Funding

National Cancer Institute, R37CA276285, (S.S.)
American Lung Association, Lung Cancer Discovery Award (S.S.)
V Foundation, Bob Bast Translational Research Grant (S.S.)
Cancer Center Support Grant, P30 CA015704 (S.S.)
Lyell Immunopharma, Sponsored Research Agreement (S.S.)
National Institutes of Health, T32 5T32GM007266-46 (A.J.S.).

Author Contributions

A.J.S and S.S. conceived the study, designed experiments, and wrote the manuscript. A.J.S. performed experiments, analyzed the data, and interpreted results. C.S., A.R.W., A.L., A.E., and E.N. generated and performed analysis of spatial transcriptomic data. T.H., S.B., E.F., X.W., S.P, and S.F. performed analysis of single cell RNA-seq data. M.G.K, S.O., W.S.N., S.G., E.B., V.Z., and M.S. performed experiments and analyzed data.

Competing Interests

S.S. has served as a consultant for, held equity in, and received research funding from Lyell Immunopharma, and is an inventor on a patent ("Immunogenic chemotherapy markedly enhances the efficacy of ROR1 CAR T cells in lung adenocarcinoma"; PCT/US2018/049812) filed by Fred Hutchinson Cancer Center and licensed by Lyell Immunopharma. X.W. and S.P. are employees and shareholders of Lyell Immunopharma. E.W.N. is a co-founder, advisor, and shareholder of ImmunoScape and is an advisor for Neogene Therapeutics. The remaining authors declare no competing interests.

Data and Materials Availability

Xenium spatial transcriptomic data are deposited in Zenodo and can be accessed under DOI: 10.5281/zenodo.14775896 (or at zenodo.org/records/14775896). Single cell RNAseq (scRNAseq) data are deposited in the Gene Expression Omnibus under the accession number GSE288687. Further information and requests for resources and reagents should be directed to and will be fulfilled by the Corresponding Author, Shivani Srivastava (ssrivas2@fredhutch.org).

1400 **Figures**

1401

1402 **Fig. 1. ROR1 CAR-T cells fail to maintain a Tcf1$^+$ reservoir within lung tumors and are not**
1403 **enhanced by PD-L1 blockade.** A) Schematic of retroviral constructs used to engineer murine
1404 ROR1 CAR-T and control T cells. TM = transmembrane. tCD19 = truncated murine CD19. B)
1405 Frequency (left), PD-1 and TIM-3 expression (middle), and IFNγ production upon *ex vivo*
1406 restimulation with PMA and ionomycin (right) by infused CD8$^+$CD19$^+$ T cells in lungs 8 days post-
1407 infusion into KP^{ROR1} mice. N=3-6 mice per group. Unpaired Student's two-way t-test. C)
1408 Representative flow plots (left) and summary (right) of Tcf1 and PD-1 expression by CD8$^+$CD19$^+$
1409 CAR-T cell over time *in vivo*. N=5 mice per group. One-way ANOVA with Tukey's post-test. D)
1410 PD-L1 expression on CD11b$^+$Ly6G$^+$ neutrophils and CD11c$^+$F4/80$^+$ macrophages within KP^{ROR1}
1411 lung tumors 8 days post-treatment with control T cells or ROR1 CAR-T cells. N=3-6 mice per
1412 group. Unpaired Student's two-way t-test. E) ROR1 CAR-T cell number (left) and PD-1 expression
1413 (right) 14 and 35 days post-infusion into KP^{ROR1} mice and treatment with vehicle or anti-PD-L1.
1414 N=5-6 mice per group. Unpaired Student's two-way t-test. F) Representative IHC staining for
1415 ROR1 on lungs of KP^{ROR1} mice 45 days post-infusion with ROR1 CAR-T cells +/- anti-PD-L1. G)
1416 Quantification of ROR1$^+$ tumor from IHC images of KP^{ROR1} lungs treated as indicated 45 days
1417 post-infusion. N=6-7 mice per group. Unpaired Student's two-way t-test. Data are representative
1418 of 2 independent experiments.

1419

1420 **Fig. 2. Overexpression of AP-1 family TFs affects maintenance of intratumoral Tcf1$^+$ CAR-**
1421 **T cells and long-term persistence *in vivo*.** A) Schematic of ROR1 CAR, cJun.ROR1 CAR, and
1422 BATF.ROR1 CAR retroviral constructs used to generate murine CAR-T cells. TM =
1423 transmembrane. tCD19 = truncated murine CD19. B) Tcf1 expression (left) and accumulation
1424 (right) of CD8$^+$GFP$^+$ CAR-T cells in infusion products (**IP**) and within tumors 8 days post-infusion
1425 into B6 mice transplanted with KP-ROR1 lung tumors. One-way ANOVA with Tukey's post-test.
1426 N=5-6 mice per group. C) Survival of B6 mice transplanted with KP-ROR1 lung tumors and treated
1427 with Cy and indicated CAR-T cells. Log-rank Mantel-Cox test. N=4-5 mice per groups. D)
1428 Treatment scheme showing co-infusion of CAR-T cells. KP = Kras$^{LSL-G12D/+}$p53$^{f/f}$. I.T =
1429 intratracheal. Cy = cyclophosphamide. E) Frequency of CD45.1$^+$CD8$^+$GFP$^+$ ROR1 (pink) and
1430 CD45.2$^+$CD8$^+$GFP$^+$ cJun.ROR1 CAR-T cells (teal) of total live cells in spleens or lungs from non-
1431 tumor bearing WT or tumor-bearing KP^{ROR1} mice 8 and 22 days post-CAR-T cell infusion. Lines
1432 indicate paired comparisons between ROR1 CAR-T and cJun.ROR1 CAR-T cells in the same

1433 mice. N=3-6 mice per group. Paired Student's two-way t-test. F) Treatment scheme showing
1434 separate CAR-T infusion. G) Frequency of $CD8^+GFP^+$ ROR1 (pink) and cJun.ROR1 CAR-T cells
1435 (teal) of total live cells in lungs of tumor-bearing KP^{ROR1} mice 8 and 35 days post-CAR-T cell
1436 infusion. N=5-9 mice per group. Unpaired Student's two-way t-test. H) Representative IHC
1437 staining for CD8 on lungs of KP^{ROR1} mice 21 days post-infusion with ROR1 CAR-T or cJun.ROR1
1438 CAR-T cells. Yellow line indicates tumor margin. I) IHC analysis showing quantification of $CD8^+$
1439 cells at various distances from tumor margin in KP^{ROR1} lungs 21 days post-infusion of ROR1 CAR-
1440 T or cJun.ROR1 CAR-T cells. Two-way ANOVA with Tukey's post-test. N=3 mice per group. Data
1441 are representative of 2-5 independent experiments.
1442
1443

1444 **Fig. 3. c-Jun overexpression improves preservation of stem-like PD-1^+Tcf1^+ CAR-T cells**
1445 **within lung tumors in a cell-intrinsic manner.** A) Unsupervised clustering of ROR1 and
1446 cJun.ROR1 CAR-T cells from the Infusion Product or from KP^{ROR1} tumors 9 and 30 days post-
1447 infusion and analyzed by scRNA-seq. B) Clusters in (A) colored by time point. C) Dot plot showing
1448 expression of genes that define each CAR-T cell subcluster. D) Geneset scores of enriched
1449 pathways from Jansen et al.[53] in CAR-T cell subclusters. E) Clusters in (A) colored by CAR-T cell
1450 product. F) K-nearest neighbor graph using Milo showing neighborhoods enriched in cJun.ROR1
1451 CAR-Ts (teal) or ROR1 CAR-Ts (pink). G) Differential abundance analysis using Milo showing
1452 fold change enrichment of neighborhoods within specific CAR-T subclusters in either cJun.ROR1
1453 CAR-Ts (teal) or ROR1 CAR-Ts (pink). H) Heatmap showing genes differentially expressed
1454 between neighborhoods enriched in ROR1 CAR-T or cJun.ROR1 CAR-T cells. I, J)
1455 Representative flow cytometry plots (I) and summary (J) showing frequency of Tcf1^+TIM-3^- stem-
1456 like subset among $CD8^+GFP^+PD\text{-}1^+$ CAR-T cells in KP^{ROR1} lungs 9 and 30 days post-infusion.
1457 N=3-4 mice per group. Two-way ANOVA with Tukey's post-test. K) Frequency of Tcf1^+TIM-3^-
1458 stem-like cells among $CD45.1^+CD8^+GFP^+PD\text{-}1^+$ ROR1 CAR-T (pink) and $CD45.2^+CD8^+GFP^+PD\text{-}$
1459 1^+ cJun.ROR1 CAR-T cells (teal) in KP^{ROR1} lungs 9 days post-co-infusion. Lines indicated
1460 matched ROR1 and cJun.ROR1 CAR-T cells within the same mice. N=6 mice per group. Paired
1461 Student's two-way t-test. Data are representative of 2 independent experiments.
1462
1463

1464 **Fig. 4. cJun.ROR1 CAR-T cells show improved function but ultimately exhaust *in vivo*.** A,
1465 B): Representative flow cytometry plots (A) and summary (B) of inhibitory receptor expression on
1466 $CD8^+GFP^+$ ROR1 CAR-T (pink) and cJun.ROR1 CAR-T cells (teal) from KP^{ROR1} lungs 9 days and

1467 30 days post-infusion. N=3-5 mice per group. Unpaired Student's two-way t-test. C, D)
1468 Representative flow cytometry plots (C) and summary (D) of intracellular cytokine staining of
1469 $CD8^+GFP^+$ ROR1 CAR-T (pink) and cJun.ROR1 CAR-T cells (teal) in KP^{ROR1} lungs 8 and 35 days
1470 post-infusion after *ex vivo* restimulation with PMA and ionomycin. N=5-9 mice per group. Unpaired
1471 Student's two-way t-test. E, F) Representative flow cytometry plots (E) and summary (F) of Tox
1472 expression in $CD8^+GFP^+$ ROR1 CAR-T (pink) and cJun.ROR1 CAR-T cells (teal) in KP^{ROR1} lungs
1473 9 and 30 days post-infusion. N=3-5 mice per group. Two-way ANOVA with Tukey's post-test. Data
1474 are representative of 2-5 independent experiments.
1475
1476 **Fig. 5. c-Jun overexpression dramatically sensitizes ROR1 CAR-T cells to enhancement**
1477 **with PD-L1 blockade.** A) Treatment schematic. I.T. = intratracheal. Cy = cyclophosphamide. B)
1478 Representative flow cytometry plots showing expression of the CAR transduction marker (GFP)
1479 and PD-1 in $CD8^+$ T cells from KP^{ROR1} lungs 5 days post-infusion. C) Absolute number and PD-1
1480 expression in $CD8^+GFP^+$ CAR-T cells (top) and $CD8^+GFP^-$ endogenous T cells (bottom) in lungs
1481 of KP^{ROR1} mice treated as indicated. N=4-5 mice per group. One-way ANOVA with Tukey's post-
1482 test. D) Representative flow cytometry plots showing Tcf1 and TIM-3 expression in $CD8^+GFP^+PD$-
1483 1^+ CAR-T cells in KP^{ROR1} lungs 5 days post-infusion. E) Frequency of $Tcf1^+TIM\text{-}3^-$ stem-like
1484 precursor exhausted (**Tpex**) and $Tcf1^-TIM\text{-}3^+$ terminally exhausted (**Tex**) subsets of
1485 $CD8^+GFP^+PD\text{-}1^+$ CAR-T cells in KP^{ROR1} lungs 5 days post-infusion. N=4-5 mice per group. One-
1486 way ANOVA with Tukey's post-test. Data are representative of 2 independent experiments
1487
1488 **Fig. 6. c-Jun levels are downregulated post-transcriptionally in cJun.ROR1 CAR-T cells**
1489 **and restored by PD-L1 blockade.** A) Flow cytometry plots showing murine c-Jun expression in
1490 ROR1 CAR-T (pink) and cJun.ROR1 CAR-T cells (teal) pre-infusion and within KP^{ROR1} lungs 9
1491 days post-infusion. B) Frequency of c-Jun (left) and ratio of c-Jun to GFP median fluorescence
1492 intensity (**MFI**) (right) in $CD8^+GFP^+$ CAR-T cells in the infusion product (**IP**) and in KP^{ROR1} lungs 9
1493 days post-infusion. N=3-5 mice per group. Two-way ANOVA with Tukey's post-test. C) Schematic
1494 of retroviral CAR and c-Jun constructs. D) Total c-Jun expression in $CD8^+GFP^+$ CAR-T cells in
1495 the IP or in KP^{ROR1} lungs 8 days post-infusion. N=5 mice per group. Two-way ANOVA with Tukey's
1496 post-test. E) Total c-Jun expression in $CD8^+GFP^+Thy1.1^+$ CAR-T cells co-transduced with ROR1
1497 CAR-P2A-tCD19/GFP and cJun-P2A-Thy1.1 vectors in the IP and in KP^{ROR1} lungs 8 days post-
1498 infusion. N=5 mice per group. Unpaired Student's two-way t-test. F) Summary (left) and
1499 representative flow cytometry plot (right) of c-Jun expression in $CD8^+GFP^+$ ROR1 CAR-T (pink)
1500 and cJun.ROR1 CAR-T cells (teal) in KP^{ROR1} lungs 5 days post-infusion and treatment with vehicle

1501 (filled) or αPD-L1 antibody (unfilled). N=4-5 mice per group. One-way ANOVA with Tukey's post-
1502 test. G) PD-1 expression on CRISPR/Cas9 mock-edited and PD-1^{KO} cJun.ROR1 CAR-T cell
1503 infusion products 24 hr post-stimulation with PMA/ionomycin. N=3 technical replicates. Unpaired
1504 Student's two-way t-test. H) c-Jun levels in tumor-infiltrating cJun.ROR1 CAR-T cells treated as
1505 indicated 9 days post-infusion into B6 mice bearing transplanted KP^{ROR1} tumors. N=5-6 mice per
1506 group. One-way ANOVA with Tukey's post-test. I) c-Jun levels in mock-edited and PD-1^{KO}
1507 cJun.ROR1 CAR-T cells 9 days post-co-infusion into tumor-bearing KP^{ROR1} mice. N=4 mice per
1508 group. Paired Student's two-way t-test. Data are representative of 2 independent experiments.
1509

1510 **Fig. 7. cJun.ROR1 CAR-Ts localize more closely to PD-L1^{+} cells and show reduced terminal**
1511 **differentiation in response to PD-L1 blockade.** A) Unsupervised clustering of spatial
1512 transcriptomic profiles of cells from lungs of KP^{ROR1} mice 7 days post-treatment with ROR1 CAR-
1513 T or cJun.ROR1 CAR-T cells +/- anti-PD-L1. N=1 lung per treatment group. B) Spatial plot
1514 showing localization of *ROR1_CART*$^{+}$ cells (black) in tumor (red), airway/blood vessels (blue),
1515 and normal lung parenchyma (grey). C) Proportion of cells in indicated spatial regions of each
1516 sample expressing the *ROR1_CART* transgene. CAR-T frequency was calculated within each
1517 individual tumor nodule. N=8-35 tumor nodules from 1 lung per group. One-way ANOVA with
1518 Tukey's post-test. D) Pie chart showing proportion of each cluster in (A) within tumor region of
1519 each sample. E) Left: Proportion of various myeloid clusters among total cells in each tumor
1520 nodule. N=8-35 tumor nodules from 1 lung per group. One-way ANOVA with Tukey's post-test.
1521 F) Left: Representative image illustrating proximity analysis calculation. Red = cells co-expressing
1522 *ROR1_CART* and *Pdcd1* (PD-1^{+} CAR-T cells). Blue = cells expressing *Cd274* (PD-L1^{+} cells).
1523 Right: mean number of PD-L1^{+} neighbors within a 20um radius of a PD-1^{+} CAR-T cell in each
1524 tumor nodule. N=17-35 tumor nodules from 1 lung per group. G) Sub-clustering of CAR-T cells.
1525 H) Dot plot showing expression of genes defining each cluster. I) Proportion of indicated CAR-T
1526 subcluster among total cell within each tumor nodule. N=8-35 tumor nodules from 1 lung per
1527 group. One-way ANOVA with Tukey's post-test. J) Distance of indicated CAR-T subset from tumor
1528 border normalized by tumor radius. Connecting lines indicate Tpex and Teff CAR-T subsets within
1529 the same tumor nodule. Paired Student's two-way t-test. N=8-35 tumor nodules from 1 lung per
1530 group.
1531

1532 **Fig. 8. c-Jun overexpression overcomes resistance of ROR1 CAR-T cells to PD-L1**
1533 **blockade.** A) Treatment schematic. I.T. = intratracheal. Cy = cyclophosphamide. B)
1534 Representative IHC staining for ROR1 on lungs of KP^{ROR1} mice 42 days post-infusion with ROR1

1535 CAR-T or cJun.ROR1 CAR-T cells. +/- anti-PD-L1. C) Quantification of ROR1^{+} tumor (top) and
1536 total tumor (bottom) from IHC images of KP^{ROR1} lungs treated as indicated 42 days post-infusion.
1537 N=3-7 mice per group. One-way with ANOVA with Tukey's post-test. D) Treatment schematic. E)
1538 Left: ROR1 expression on KP-ROR1 tumor cell lines derived from GEM model and sorted to be
1539 >95% ROR1^{+}. Right: representative IHC showing ROR1 expression on lungs of B6 mice
1540 transplanted with KP-ROR1 lung tumors 21 days post-tumor injection and pre-CAR-T cell
1541 infusion. F) Representative flow plots showing GFP and PD-1 expression on CD8^{+} T cells within
1542 lung tumors 14 days post-infusion. G) Absolute number of CD8^{+}GFP^{+} CAR-T cells and CD8^{+}PD-
1543 1^{+} endogenous T cells within lung tumors 14 days post-infusion. N=6-7 mice per group. One-way
1544 ANOVA with Tukey's post-test. H) Survival. Log-rank Mantel-Cox test. N=7-8 mice per group.
1545 Data are representative of 2 independent experiments.

1546 **Supplemental Information**
1547
1548 **Supplementary Fig. 1. Modification of the lentiviral hROR1-Cre vector improves co-**
1549 **expression of hROR1 and Cre recombinase.** A) Schematic of lentiviral constructs used to
1550 induce tumors in KP mice. ffluc = firefly luciferase. hROR1t = truncated human ROR1. Cre =
1551 Cre recombinase. B) Flow cytometry plots showing expression of hROR1 in GFP^+ $3TZ^{LSL\text{-}GFP}$
1552 "GreenGo" Cre-reporter cells infected with the indicated lentiviruses. C) Representative IHC
1553 staining (left) and summary (right) of ROR1 expression on lung tumors in KP mice infected with
1554 Cre or hROR1-Cre lentivirus. Data are representative of 3-5 independent experiments.
1555
1556 **Supplementary Fig. 2. Overexpression of AP-1 family TFs does not substantially alter**
1557 **ROR1 CAR-T cell function prior to infusion**. A) Flow cytometry plots showing ROR1 CAR, c-
1558 Jun, and BATF expression in $CD8^+$ T cells untransduced or transduced with ROR1 CAR,
1559 cJun.ROR1 CAR, or BATF.ROR1 CAR vectors prior to infusion. B) Flow cytometry plot showing
1560 Tcf1 expression in CAR-T cell infusion products relative to ROR1 CAR-T cells within KP^{ROR1}
1561 tumors 8 days post-infusion (grey). C) Proliferation of CAR-T cells 72 hours post-stimulation with
1562 PMA and ionomycin *in vitro*. N=3 technical replicates. Two-way ANOVA with Tukey's post-test.
1563 D) Representative plot showing dilution of Cell Trace Blue dye upon stimulation with PMA and
1564 ionomycin in $CD8^+GFP^+$ CAR-T cell infusion product. E) Intracellular cytokine staining analysis of
1565 $CD8^+GFP^+$ CAR-T cell infusion products upon stimulation with PMA and ionomycin *in vitro*. One-
1566 way ANOVA with Tukey's post-test. Data are representative of 3 independent experiments.
1567
1568 **Supplementary Fig. 3. Sub-clustering of CAR-T cells from single cell RNA-seq data.** A)
1569 Unsupervised clustering (left) and *Cd3e* expression (right) of CAR-T infusion product and $CD8^+$
1570 cells enriched from KP^{ROR1} tumors 9 and 30 days post-CAR-T infusion. B) Expression of *Rag1*
1571 among clusters in (A). C) Coloring of clusters in (A) by sample hash. N = 3 mice per group. D)
1572 Sub-clustering of cells expressing *Cd3e* and excluding *Rag1* (left) and expression of *Cd3e*
1573 (middle) and *CAR* transgene (right) among T cell subclusters. E) Sub-clustering of CAR^+
1574 clusters (left) and expression of *CAR* among CAR-T subclusters (right). F, G) Enrichment of
1575 various gene sets for memory/stem-like T cells (F) or terminally exhausted T cells (G) among
1576 CAR-T subclusters.
1577
1578 **Supplementary Fig. 4. c-Jun overexpression improves activity of both ROR1.BBζ and**
1579 **ROR1.28ζ CAR-T cells, but tumors ultimately progress.** A) Frequency of GFP^+ CAR-T cells of

1580 $CD8^+$ T cells in lungs 8 days post-infusion into B6 mice bearing transplanted KP-ROR1 lung
1581 tumors. N=3-4 mice per group. One-way ANOVA with Tukey's post-test. B, C) Inhibitory receptor
1582 expression (B) and cytokine production upon *ex vivo* restimulation with PMA and ionomycin (C)
1583 in $CD8^+GFP^+$ CAR-T cells in lungs 8 days post-infusion into B6 mice bearing transplanted KP^{ROR1}
1584 lung tumors. N=3-4 mice per group. One-way ANOVA with Tukey's post-test. D) Survival of B6
1585 mice bearing transplanted KP^{ROR1} tumors and treated with the indicated T cell products. N=4 mice
1586 per group. Log-rank Mantel-Cox test. Data are representative of 2 independent experiments.
1587
1588 **Supplementary Fig. 5. Annotation of TME single cell RNAseq clusters.** A) Unsupervised
1589 clustering of live cells sorted from KP^{ROR1} tumors of mice left untreated, or 9 or 30 days post-
1590 infusion with ROR1 CAR-T or cJun.ROR1 CAR-T cells. B, C) Clusters in (A) colored by time point
1591 (B) or treatment group (C). D) Dot plot showing expression of various lineage-defining genes
1592 across clusters in (A). E,F) UMAP (E) and violin plot (F) showing expression of *Cd274* (encodes
1593 PD-L1) across clusters in (A). G) Expression of PD-L1 on $CD45^-EpCAM^+ROR1^+$ KP tumor cells,
1594 $CD11c^+F4/80^+$ macrophages, and $CD11b^+Ly6G^+$ neutrophils within KP^{ROR1} lung tumors left
1595 untreated (black) or 9 days post-infusion of ROR1 CAR-Ts (pink) or cJun.ROR1 CAR-Ts (teal).
1596 N=3-5 mice per group. One-way ANOVA with Tukey's post-test.
1597
1598 **Supplementary Fig. 6. Annotation of 10X Xenium clusters.** Lungs from KP^{ROR1} mice were
1599 harvested 7 days post-treatment with ROR1 CAR-Ts + vehicle, ROR1 CAR-Ts + anti-PD-L1,
1600 cJun.ROR1 CAR-Ts + vehicle, or cJun.ROR1 CAR-Ts + anti-PD-L1 and analyzed by 10X
1601 Xenium. Dot plot summarizes expression of various genes defining each cluster.

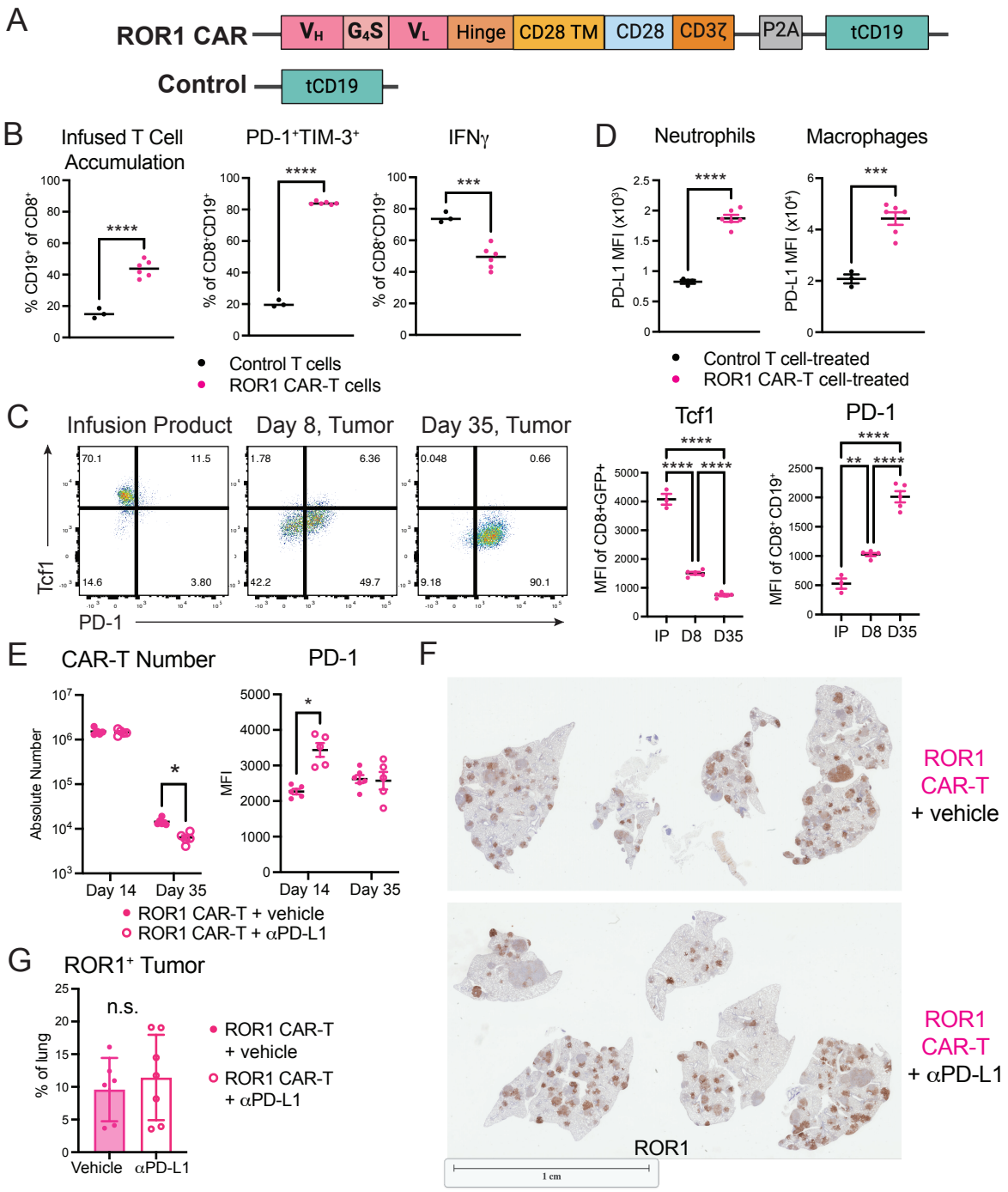

Figure 1. ROR1 CAR-T cells fail to maintain a Tcf1+ reservoir within lung tumors and are not enhanced by PD-L1 blockade. A) Schematic of retroviral constructs used to engineer murine ROR1 CAR-T and control T cells. TM = transmembrane. tCD19 = truncated murine CD19. B) Frequency (left), PD-1 and TIM-3 expression (middle), and IFNγ production upon ex vivo restimulation with PMA and ionomycin (right) by infused CD8+CD19+ T cells in lungs 8 days post-infusion into KP^{ROR1} mice. N=3-6 mice per group. Unpaired Student's two-way t-test. C) Representative flow plots (left) and summary (right) of Tcf1 and PD-1 expression by CD8+CD19+ CAR-T cell over time in vivo. N=5 mice per group. One-way ANOVA with Tukey's post-test. D) PD-L1 expression on CD11b+Ly6G+ neutrophils and CD11c+F4/80+ macrophages within KP^{ROR1} lung tumors 8 days post-treatment with control T cells or ROR1 CAR-T cells. N=3-6 mice per group. Unpaired Student's two-way t-test. E) ROR1 CAR-T cell number (left) and PD-1 expression (right) 14 and 35 days post-infusion into KP^{ROR1} mice and treatment with vehicle or anti-PD-L1. N=5-6 mice per group. Unpaired Student's two-way t-test. F) Representative IHC staining for ROR1 on lungs of KP^{ROR1} mice 45 days post-infusion with ROR1 CAR-T cells +/- anti-PD-L1. G) Quantification of ROR1+ tumor from IHC images of KP^{ROR1} lungs treated as indicated 45 days post-infusion. N=6-7 mice per group. Unpaired Student's two-way t-test. Data are representative of 2 independent experiments.

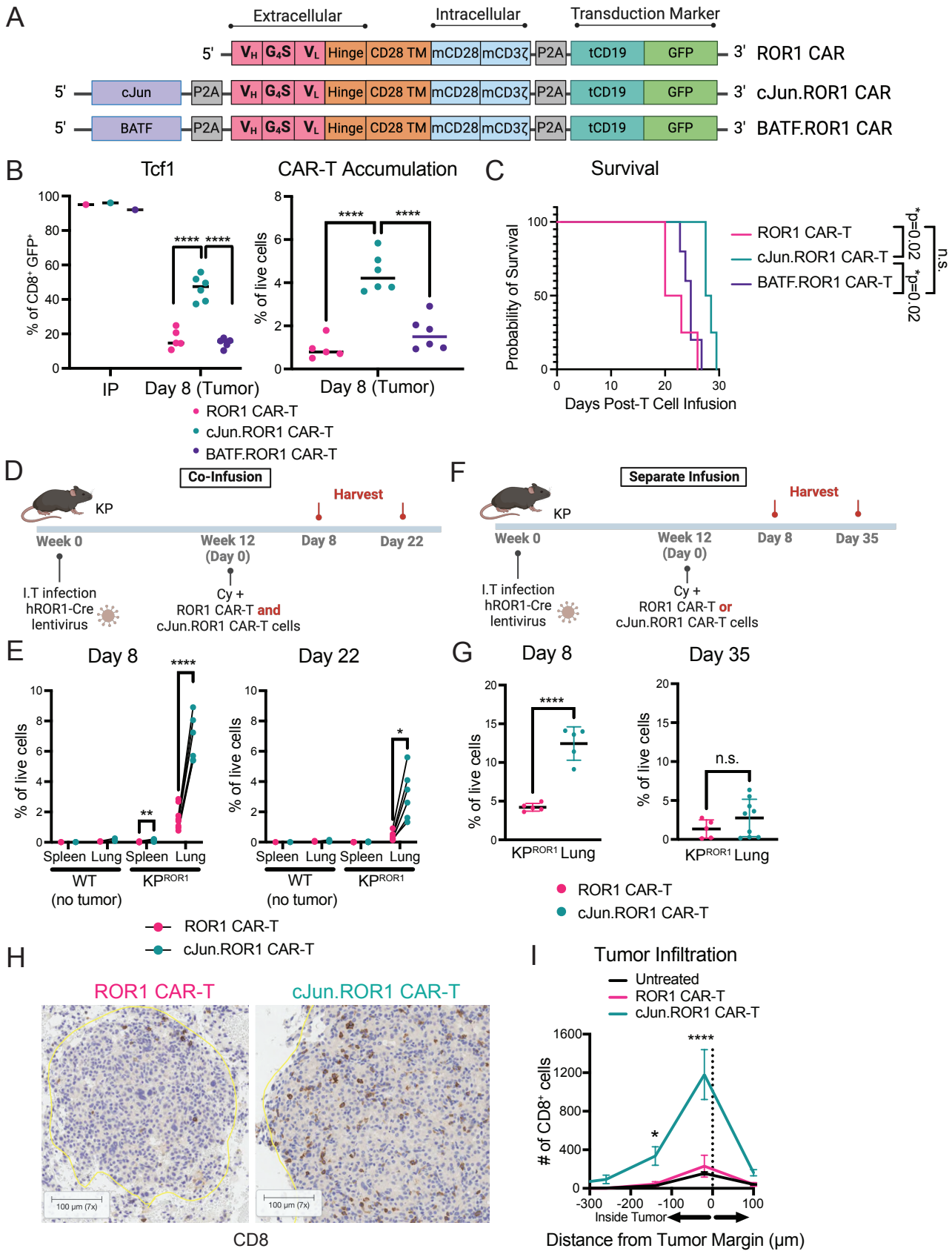

Figure 2. Overexpression of AP-1 family TFs affects maintenance of intratumoral Tcf1+ CAR-T cells and long-term persistence in vivo.

Figure 2. Overexpression of AP-1 family TFs affects maintenance of intratumoral Tcf1+ CAR-T cells and long-term persistence in vivo.

A) Schematic of ROR1 CAR, cJun.ROR1 CAR, and BATF.ROR1 CAR retroviral constructs used to generate murine CAR-T cells. TM = transmembrane. tCD19 = truncated murine CD19. B) Tcf1 expression (left) and accumulation (right) of CD8+GFP+ CAR-T cells in infusion products (IP) and within tumors 8 days post-infusion into B6 mice transplanted with KP-ROR1 lung tumors. One-way ANOVA with Tukey's post-test. N=5-6 mice per group. C) Survival of B6 mice transplanted with KP-ROR1 lung tumors and treated with Cy and indicated CAR-T cells. Log-rank Mantel-Cox test. N=4-5 mice per groups. D) Treatment scheme showing co-infusion of CAR-T cells. KP = $Kras^{LSL\text{-}G12D/+}p53^{f/f}$. I.T = intratracheal. Cy = cyclophosphamide. E) Frequency of CD45.1+CD8+GFP+ ROR1 (pink) and CD45.2+CD8+GFP+ cJun.ROR1 CAR-T cells (teal) of total live cells in spleens or lungs from non-tumor bearing WT or tumor-bearing KP^{ROR1} mice 8 and 22 days post-CAR-T cell infusion. Lines indicate paired comparisons between ROR1 CAR-T and cJun.ROR1 CAR-T cells in the same mice. N=3-6 mice per group. Paired Student's two-way t-test. F) Treatment scheme showing separate CAR-T infusion. G) Frequency of CD8+GFP+ ROR1 (pink) and cJun.ROR1 CAR-T cells (teal) of total live cells in lungs of tumor-bearing KP^{ROR1} mice 8 and 35 days post-CAR-T cell infusion. N=5-9 mice per group. Unpaired Student's two-way t-test. H) Representative IHC staining for CD8 on lungs of KP^{ROR1} mice 21 days post-infusion with ROR1 CAR-T or cJun.ROR1 CAR-T cells. Yellow line indicates tumor margin. I) IHC analysis showing quantification of CD8+ cells at various distances from tumor margin in KP^{ROR1} lungs 21 days post-infusion of ROR1 CAR-T or cJun.ROR1 CAR-T cells. Two-way ANOVA with Tukey's post-test. N=3 mice per group. Data are representative of 2-5 independent experiments.

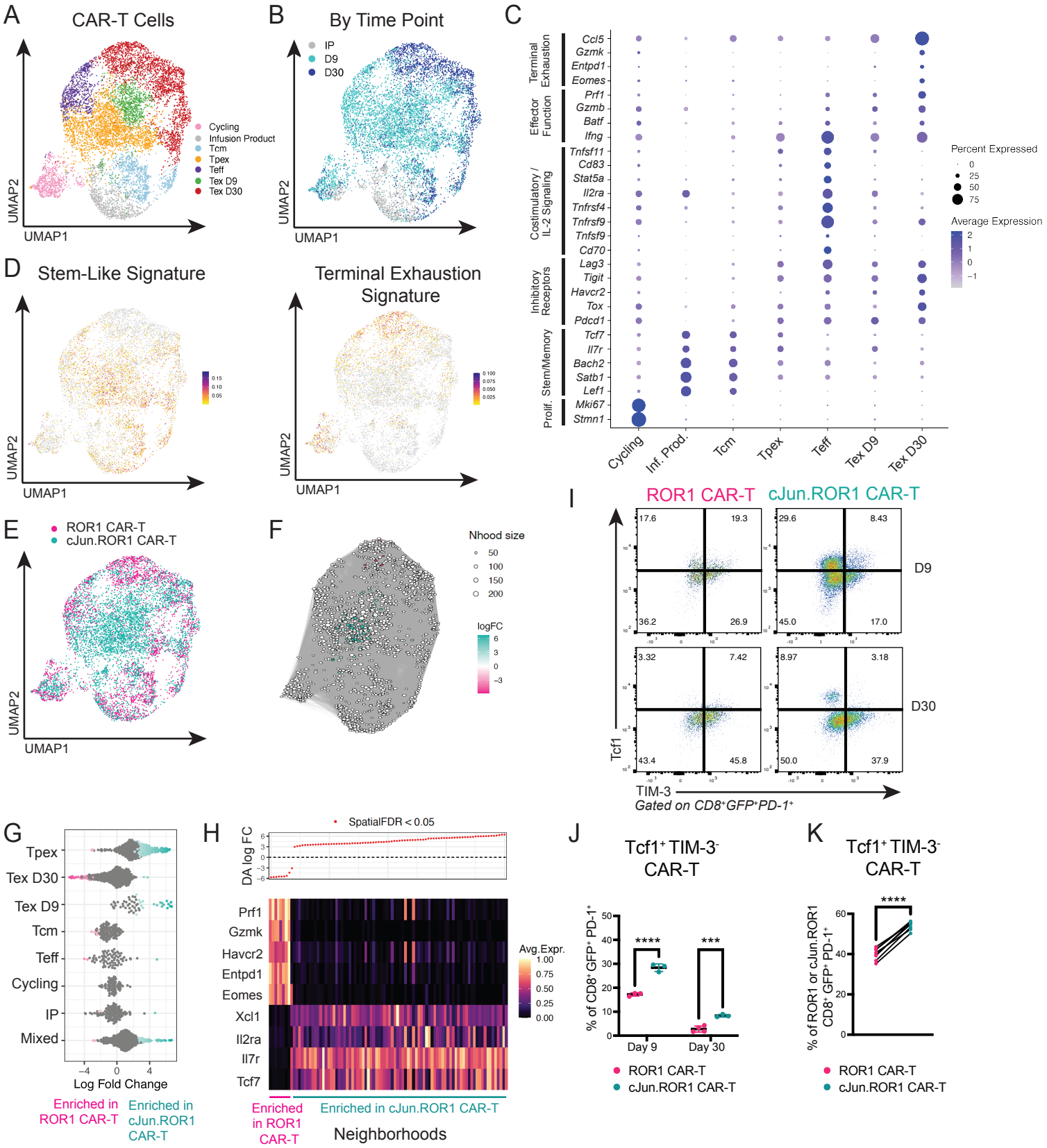

Figure 3. c-Jun overexpression improves preservation of stem-like PD-1+Tcf1+ CAR-T cells within lung tumors in a cell-intrinsic manner.

Figure 3. c-Jun overexpression improves preservation of stem-like PD-1+Tcf1+ CAR-T cells within lung tumors in a cell-intrinsic manner. A) Unsupervised clustering of ROR1 and cJun.ROR1 CAR-T cells from the Infusion Product or from KP^{ROR1} tumors 9 and 30 days post-infusion and analyzed by scRNA-seq. B) Clusters in (A) colored by time point. C) Dot plot showing expression of genes that define each CAR-T cell subcluster. D) Geneset scores of enriched pathways from Jansen et al. in CAR-T cell subclusters. E) Clusters in (A) colored by CAR-T cell product. F) K-nearest neighbor graph using Milo showing neighborhoods enriched in cJun.ROR1 CAR-Ts (teal) or ROR1 CAR-Ts (pink). G) Differential abundance analysis using Milo showing fold change enrichment of neighborhoods within specific CAR-T subclusters in either cJun.ROR1 CAR-Ts (teal) or ROR1 CAR-Ts (pink). H) Heatmap showing genes differentially expressed between neighborhoods enriched in ROR1 CAR-T or cJun.ROR1 CAR-T cells. I, J) Representative flow cytometry plots (I) and summary (J) showing frequency of Tcf1+TIM-3- stem-like subset among CD8+GFP+PD-1+ CAR-T cells in KP^{ROR1} lungs 9 and 30 days post-infusion. N=3-4 mice per group. Two-way ANOVA with Tukey's post-test. K) Frequency of Tcf1+TIM-3- stem-like cells among CD45.1+CD8+GFP+PD-1+ ROR1 CAR-T (pink) and CD45.2+CD8+GFP+PD-1+ cJun.ROR1 CAR-T cells (teal) in KP^{ROR1} lungs 9 days post-co-infusion. Lines indicated matched ROR1 and cJun.ROR1 CAR-T cells within the same mice. N=6 mice per group. Paired Student's two-way t-test. Data are representative of 2 independent experiments.

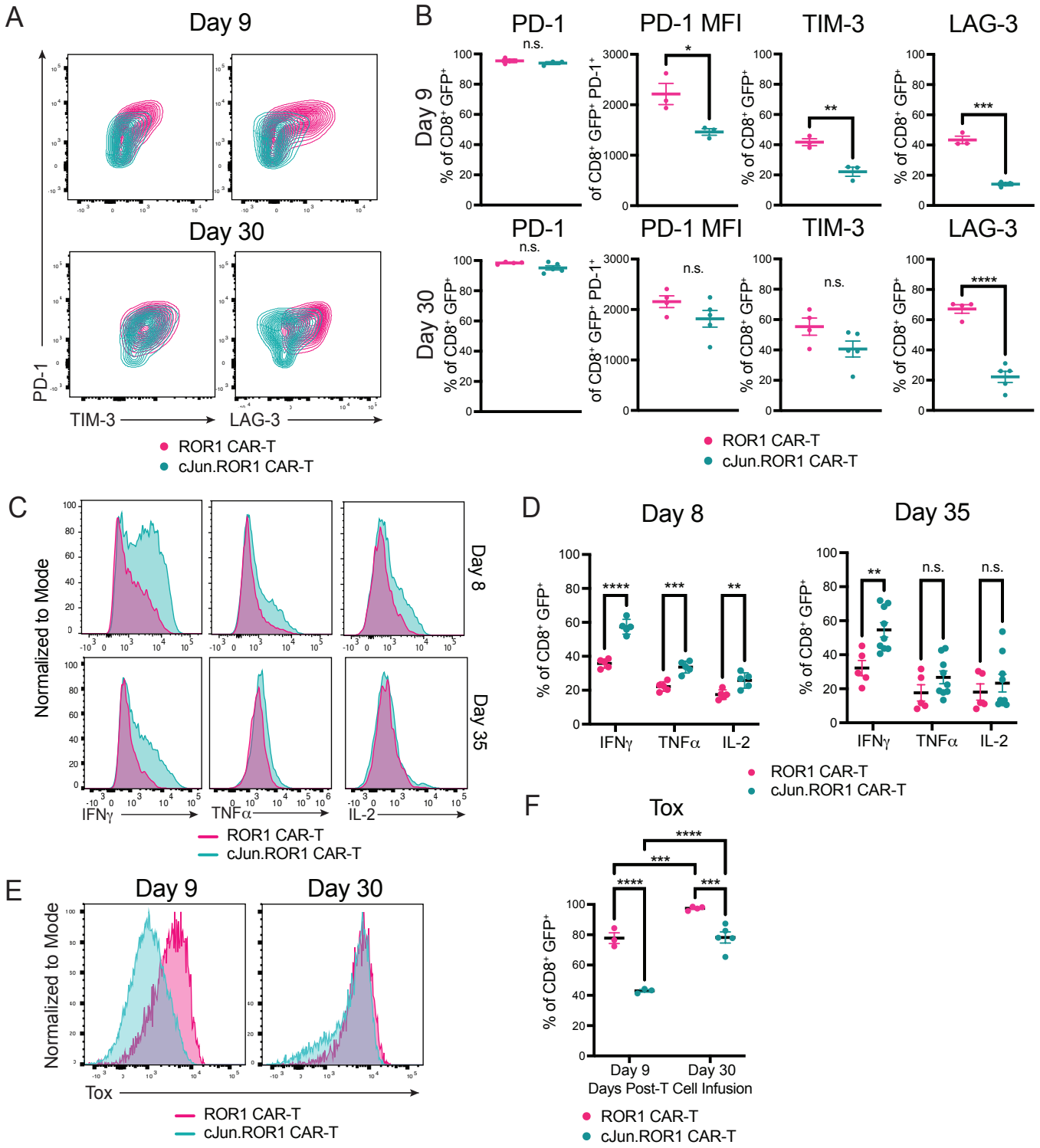

Figure 4. cJun.ROR1 CAR-T cells show improved function but ultimately exhaust *in vivo*. A, B): Representative flow cytometry plots (A) and summary (B) of inhibitory receptor expression on CD8+GFP+ ROR1 CAR-T (pink) and cJun.ROR1 CAR-T cells (teal) from KP^{ROR1} lungs 9 days and 30 days post-infusion. N=3-5 mice per group. Unpaired Student's two-way t-test. C, D) Representative flow cytometry plots (C) and summary (D) of intracellular cytokine staining of CD8+GFP+ ROR1 CAR-T (pink) and cJun.ROR1 CAR-T cells (teal) in KP^{ROR1} lungs 8 and 35 days post-infusion after ex vivo restimulation with PMA and ionomycin. N=5-9 mice per group. Unpaired Student's two-way t-test. E, F) Representative flow cytometry plots (E) and summary (F) of Tox expression in CD8+GFP+ ROR1 CAR-T (pink) and cJun.ROR1 CAR-T cells (teal) in KP^{ROR1} lungs 9 and 30 days post-infusion. N=3-5 mice per group. Two-way ANOVA with Tukey's post-test. Data are representative of 2-5 independent experiments.

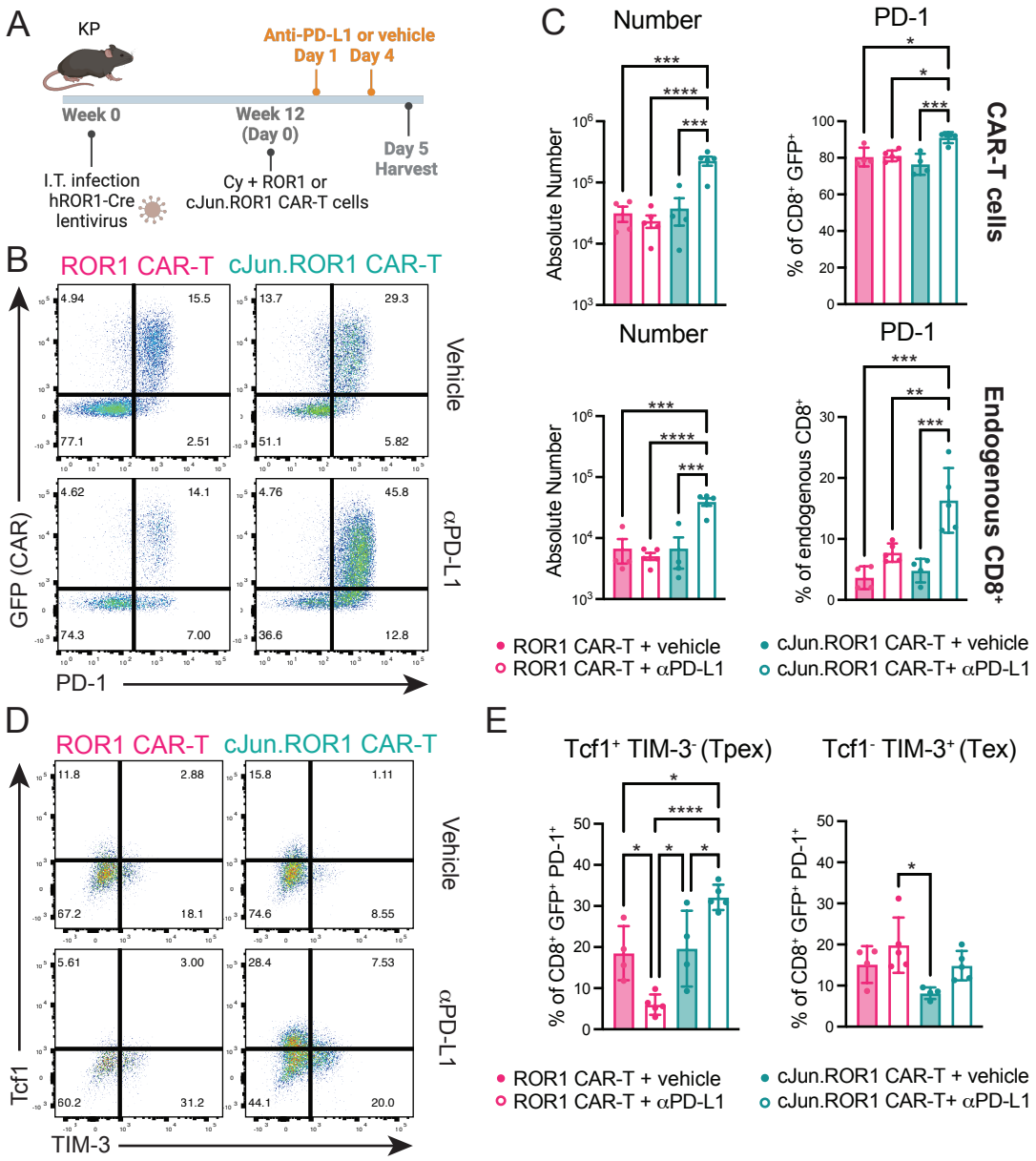

Figure 5. c-Jun overexpression dramatically sensitizes ROR1 CAR-T cells to enhancement with PD-L1 blockade. A) Treatment schematic. I.T. = intratracheal. Cy = cyclophosphamide. B) Representative flow cytometry plots showing expression of the CAR transduction marker (GFP) and PD-1 in CD8+ T cells from KP^{ROR1} lungs 5 days post-infusion. C) Absolute number and PD-1 expression in CD8+GFP+ CAR-T cells (top) and CD8+GFP- endogenous T cells (bottom) in lungs of KP^{ROR1} mice treated as indicated. N=4-5 mice per group. One-way ANOVA with Tukey's post-test. D) Representative flow cytometry plots showing Tcf1 and TIM-3 expression in CD8+GFP+PD-1+ CAR-T cells in KP^{ROR1} lungs 5 days post-infusion. E) Frequency of Tcf1+TIM-3- stem-like precursor exhausted (Tpex) and Tcf1-TIM-3+ terminally exhausted (Tex) subsets of CD8+GFP+PD-1+ CAR-T cells in KP^{ROR1} lungs 5 days post-infusion. N=4-5 mice per group. One-way ANOVA with Tukey's post-test. F) Frequency of cJun.ROR1 CAR-T cells either CRISPR/Cas9 control-edited (*Tcf7+/+*) or Tcf7-edited (*Tcf7-/-*) in lung tumors 11 days post-infusion. N=5 mice per group. Two-way ANOVA with Tukey's post-test. Data are representative of 2 independent experiments.

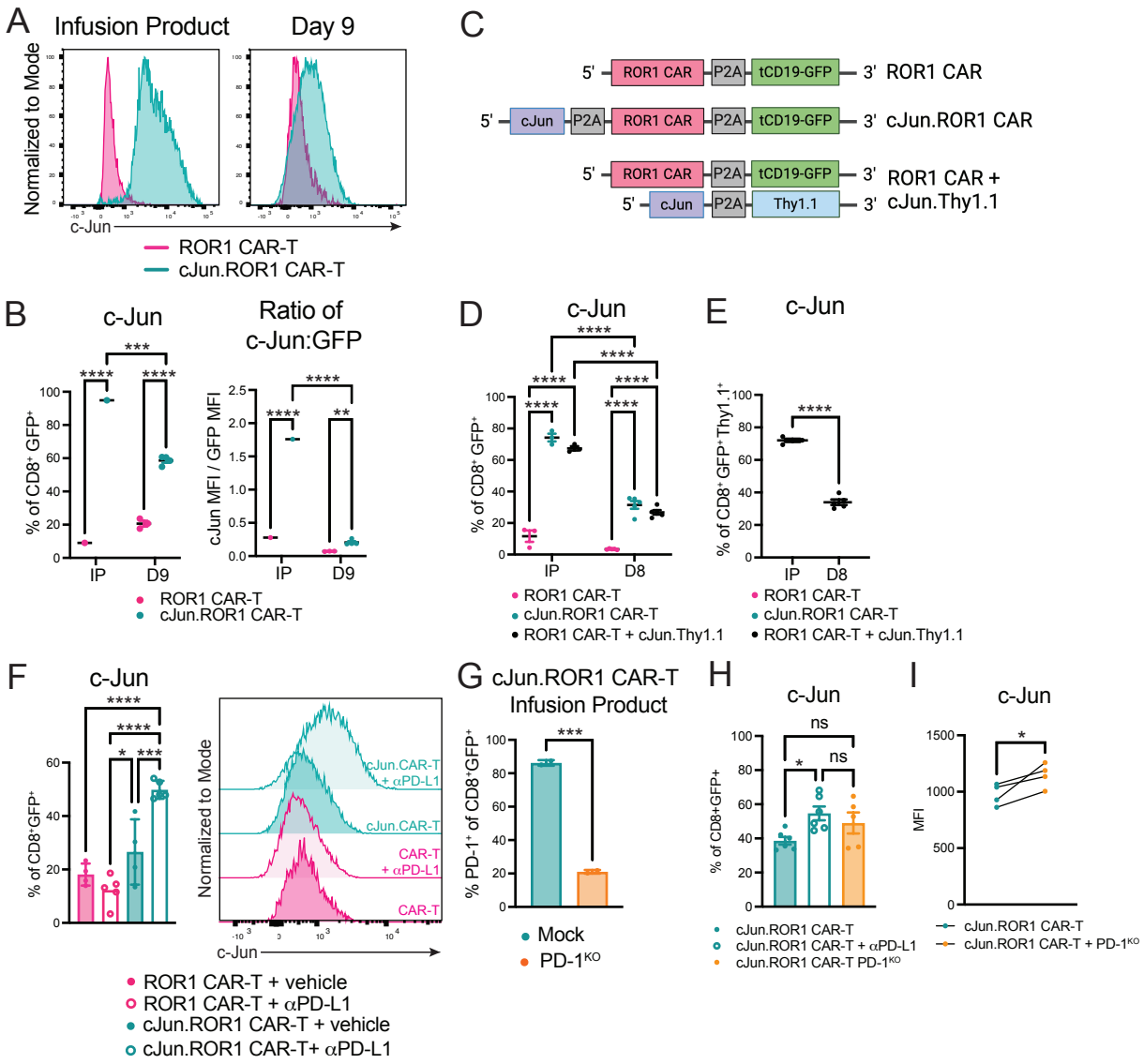

Figure 6. c-Jun levels are downregulated post-transcriptionally in cJun.ROR1 CAR-T cells and restored by PD-L1 blockade. A) Flow cytometry plots showing murine c-Jun expression in ROR1 CAR-T (pink) and cJun.ROR1 CAR-T cells (teal) pre-infusion and within KP^{ROR1} lungs 9 days post-infusion. B) Frequency of c-Jun (left) and ratio of c-Jun to GFP median fluorescence intensity (MFI) (right) in CD8+GFP+ CAR-T cells in the infusion product (IP) and in KP^{ROR1} lungs 9 days post-infusion. N=3-5 mice per group. Two-way ANOVA with Tukey's post-test. C) Schematic of retroviral CAR and c-Jun constructs. D) Total c-Jun expression in CD8+GFP+ CAR-T cells in the IP or in KP^{ROR1} lungs 8 days post-infusion. N=5 mice per group. Two-way ANOVA with Tukey's post-test. E) Total c-Jun expression in CD8+GFP+Thy1.1+ CAR-T cells co-transduced with ROR1 CAR-P2A-tCD19/GFP and cJun-P2A-Thy1.1 vectors in the IP and in KP^{ROR1} lungs 8 days post-infusion. N=5 mice per group. Unpaired Student's two-way t-test. F) Summary (left) and representative flow cytometry plot (right) of c-Jun expression in CD8+GFP+ ROR1 CAR-T (pink) and cJun.ROR1 CAR-T cells (teal) in KP^{ROR1} lungs 5 days post-infusion and treatment with vehicle (filled) or αPD-L1 antibody (unfilled). N=4-5 mice per group. One-way ANOVA with Tukey's post-test. G) PD-1 expression on CRISPR/-Cas9 mock-edited and PD-1^{KO} cJun.ROR1 CAR-T cell infusion products 24 hr post-stimulation with PMA/ionomycin. N=3 technical replicates. Unpaired Student's two-way t-test. H) c-Jun levels in tumor-infiltrating cJun.ROR1 CAR-T cells treated as indicated 9 days post-infusion into B6 mice bearing transplanted KP-ROR1 tumors. N=5-6 mice per group. One-way ANOVA with Tukey's post-test. I) c-Jun levels in mock-edited and PD-1^{KO} cJun.ROR1 CAR-T cells 9 days post-co-infusion into tumor-bearing KP^{ROR1} mice. N=4 mice per group. Paired Student's two-way t-test. Data are representative of 2 independent experiments.

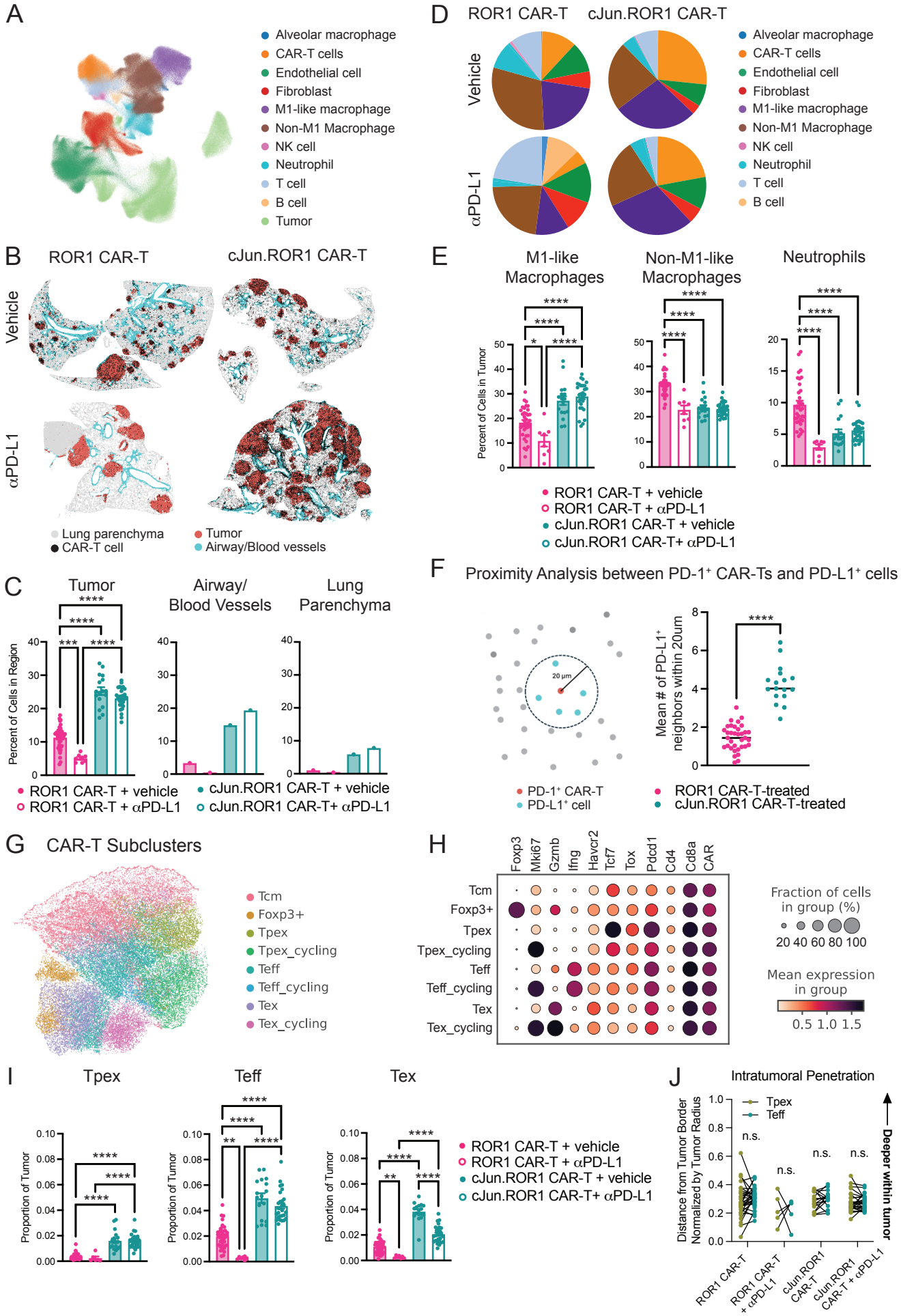

Figure 7. cJun.ROR1 CAR-Ts localize more closely to PD-L1+ cells and show reduced terminal differentiation in response to PD-L1 blockade.

Figure 7. cJun.ROR1 CAR-Ts localize more closely to PD-L1+ cells and show reduced terminal differentiation in response to PD-L1 blockade. A) Unsupervised clustering of spatial transcriptomic profiles of cells from lungs of KP^{ROR1} mice 7 days post-treatment with ROR1 CAR-T or cJun.ROR1 CAR-T cells +/- anti-PD-L1. N=1 lung per treatment group. B) Spatial plot showing localization of *ROR1_CART*+ cells (black) in tumor (red), airway/blood vessels (blue), and normal lung parenchyma (grey). C) Proportion of cells in indicated spatial regions of each sample expressing the *ROR1_CART* transgene. CAR-T frequency was calculated within each individual tumor nodule. N=8-35 tumor nodules from 1 lung per group. One-way ANOVA with Tukey's post-test. D) Pie chart showing proportion of each cluster in (A) within tumor region of each sample. E) Left: Proportion of various myeloid clusters among total cells in each tumor nodule. N=8-35 tumor nodules from 1 lung per group. One-way ANOVA with Tukey's post-test. F) Left: Representative image illustrating proximity analysis calculation. Red = cells co-expressing *ROR1_CART* and *Pdcd1* (PD-1+ CAR-T cells). Blue = cells expressing *Cd274* (PD-L1+ cells). Right: mean number of PD-L1+ neighbors within a 20um radius of a PD-1+ CAR-T cell in each tumor nodule. N=17-35 tumor nodules from 1 lung per group. G) Sub-clustering of CAR-T cells. H) Dot plot showing expression of genes defining each cluster. I) Proportion of indicated CAR-T subcluster among total cell within each tumor nodule. N=8-35 tumor nodules from 1 lung per group. One-way ANOVA with Tukey's post-test. J) Distance of indicated CAR-T subset from tumor border normalized by tumor radius. Connecting lines indicate Tpex and Teff CAR-T subsets within the same tumor nodule. N=8-35 tumor nodules from 1 lung per group. Paired Student's two-way t-test.

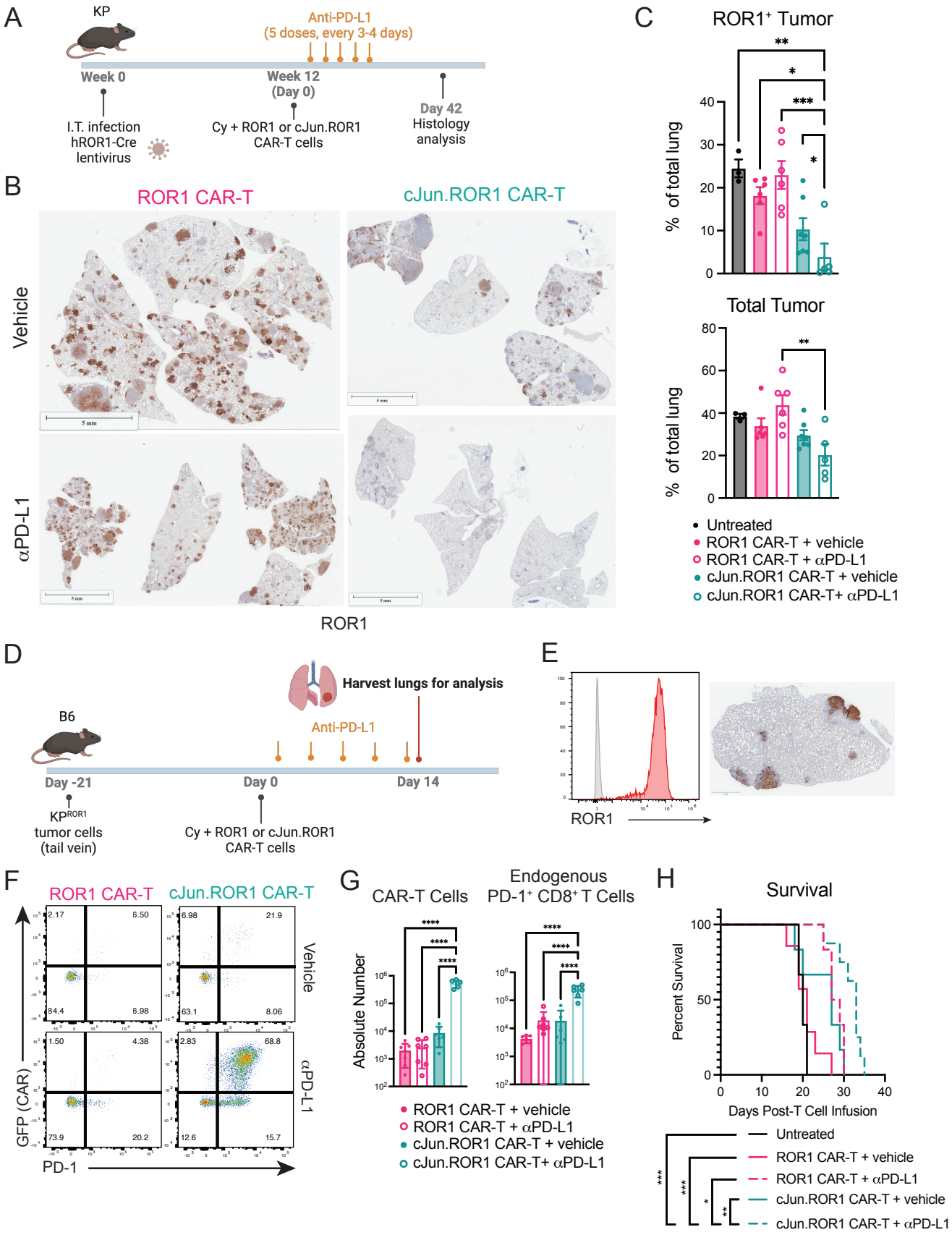

Figure 8. c-Jun overexpression overcomes resistance of ROR1 CAR-T cells to PD-L1 blockade.

Figure 8. c-Jun overexpression overcomes resistance of ROR1 CAR-T cells to PD-L1 blockade. A) Treatment schematic. I.T. = intratracheal. Cy = cyclophosphamide. B) Representative IHC staining for ROR1 on lungs of KP^{ROR1} mice 42 days post-infusion with ROR1 CAR-T or cJun.ROR1 CAR-T cells. +/- anti-PD-L1. C) Quantification of ROR1+ tumor (top) and total tumor (bottom) from IHC images of KP^{ROR1} lungs treated as indicated 42 days post-infusion. N=3-7 mice per group. One-way with ANOVA with Tukey's post-test. D) Treatment schematic. E) Left: ROR1 expression on KP-ROR1 tumor cell lines derived from GEM model and sorted to be >95% ROR1+. Right: representative IHC showing ROR1 expression on lungs of B6 mice transplanted with KP-ROR1 lung tumors 21 days post-tumor injection and pre-CAR-T cell infusion. F) Representative flow plots showing GFP and PD-1 expression on CD8+ T cells within lung tumors 14 days post-infusion. G) Absolute number of CD8+GFP+ CAR-T cells and CD8+PD-1+ endogenous T cells within lung tumors 14 days post-infusion. N=6-7 mice per group. One-way ANOVA with Tukey's post-test. H) Survival. Log-rank Mantel-Cox test. N=7-8 mice per group. Data are representative of 2 independent experiments.